Elettra Sincrotrone Trieste

ATOMIC FORCE MICROSCOPY
Imaging in Biology
Membranes

Membrane proteins

1. The residues accessible to lipid tails tend to be more hydrophobic than the residues buried inside the protein
2. Charged or polar residues can be exposed to the lipids, but they will interact either with the lipids head-groups or with other polar or charged residues of the protein
3. Polar aromatic residues (Trp, Tyr) can also interact with lipids, but tend to be located in the polar-apolar interfacial region, near the lipids carbonyls, and act as anchor for the protein in the bilayer

Examples:
the outer membrane proteins, the photosynthetic membrane proteins, the membrane transporters and channels, the respiratory enzymes, and the receptors and related proteins.

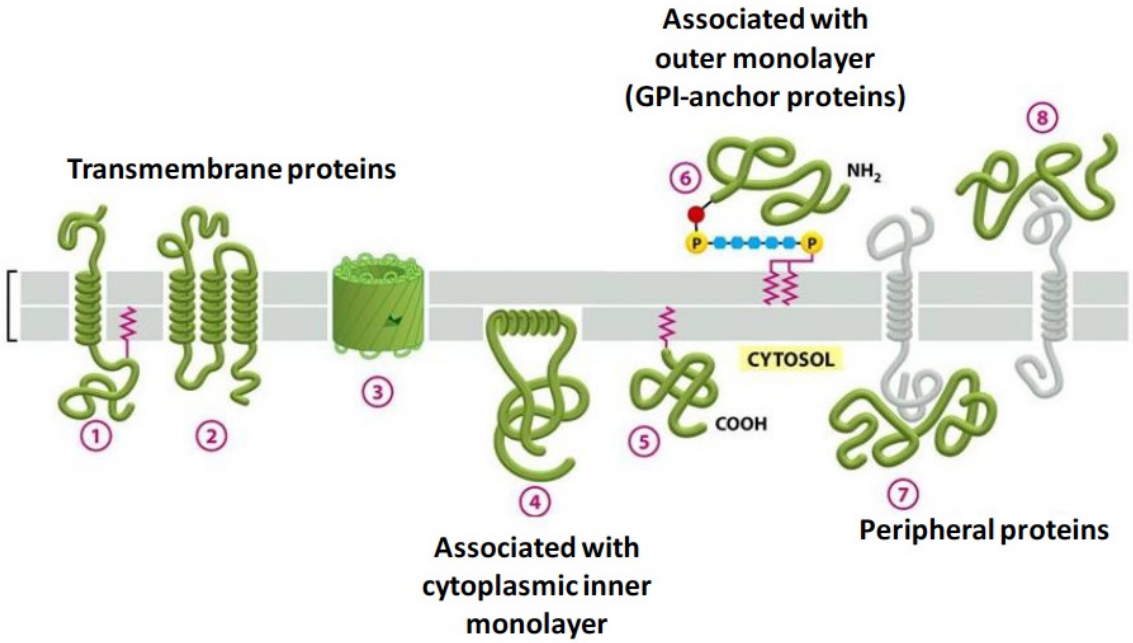

Membrane proteins

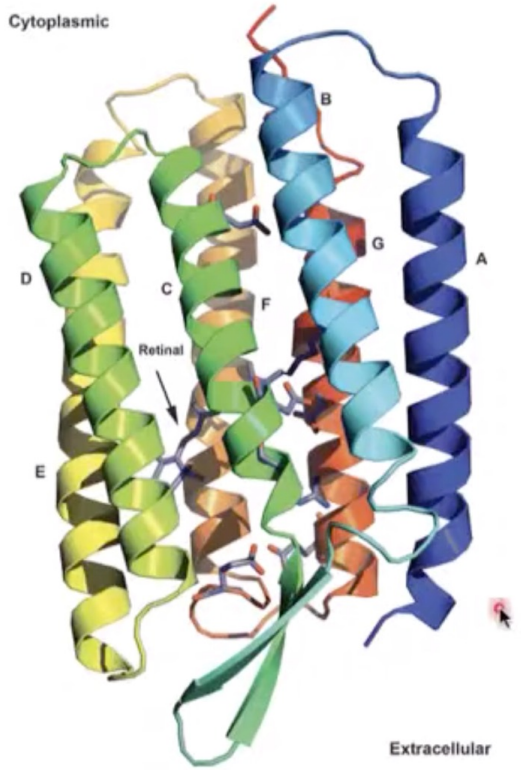

Bacteriorhodopsin
α-helical bundle

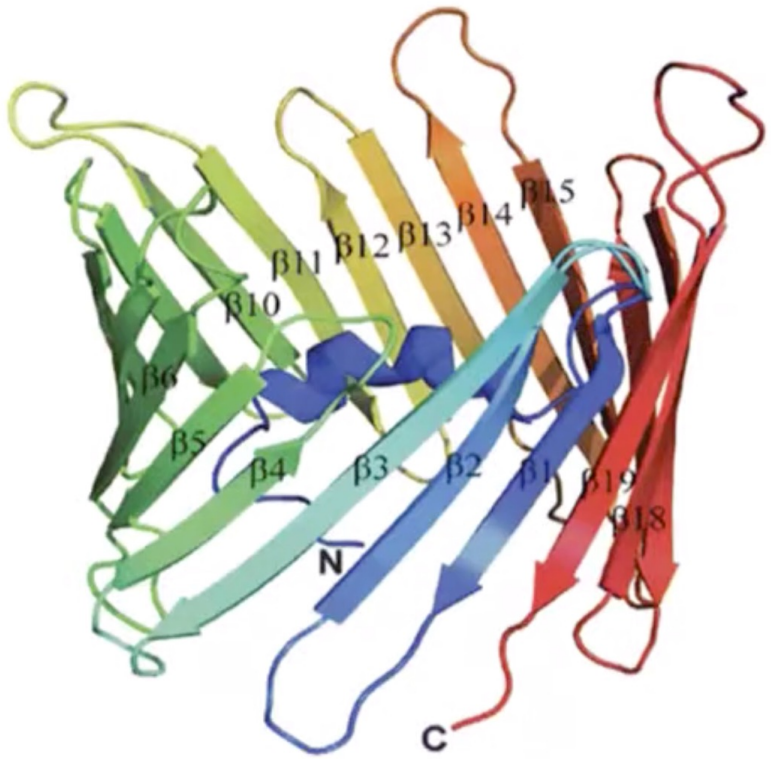

Mitochondrial porin, VDAC
β-barrel

Mary Luckey, Chapter 1:Introduction to the Structural Biology of Membrane Proteins , in *Computational Biophysics of Membrane Proteins*, 2016, pp. 1-18

Cell membranes-rafts

Tasks such as energy transduction and chemical communication between the inside and the outside of the cell are achieved by membrane proteins. However, molecular level understanding of membrane proteins function is largely hindered by the lack of structural information available, especially in biologically relevant environments

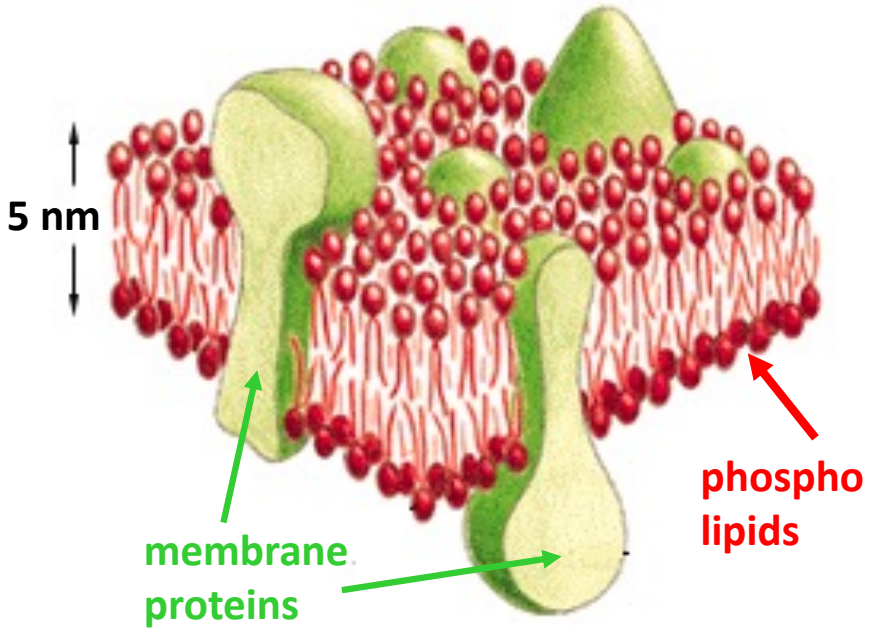

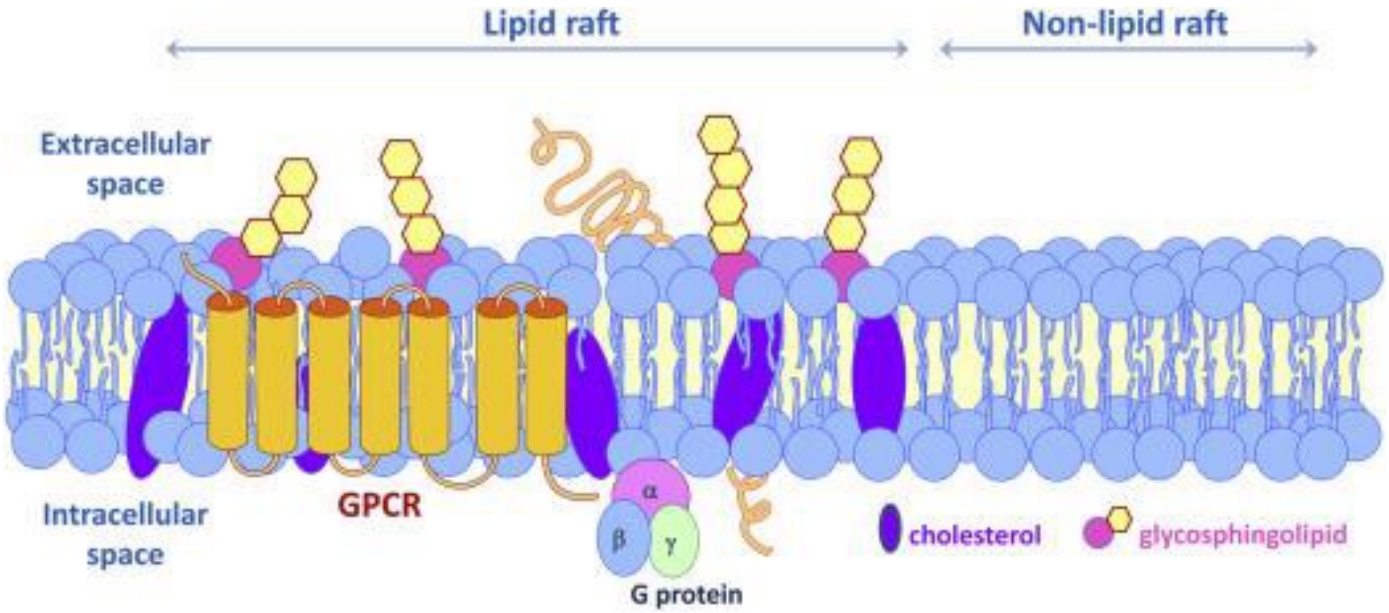

Model membranes

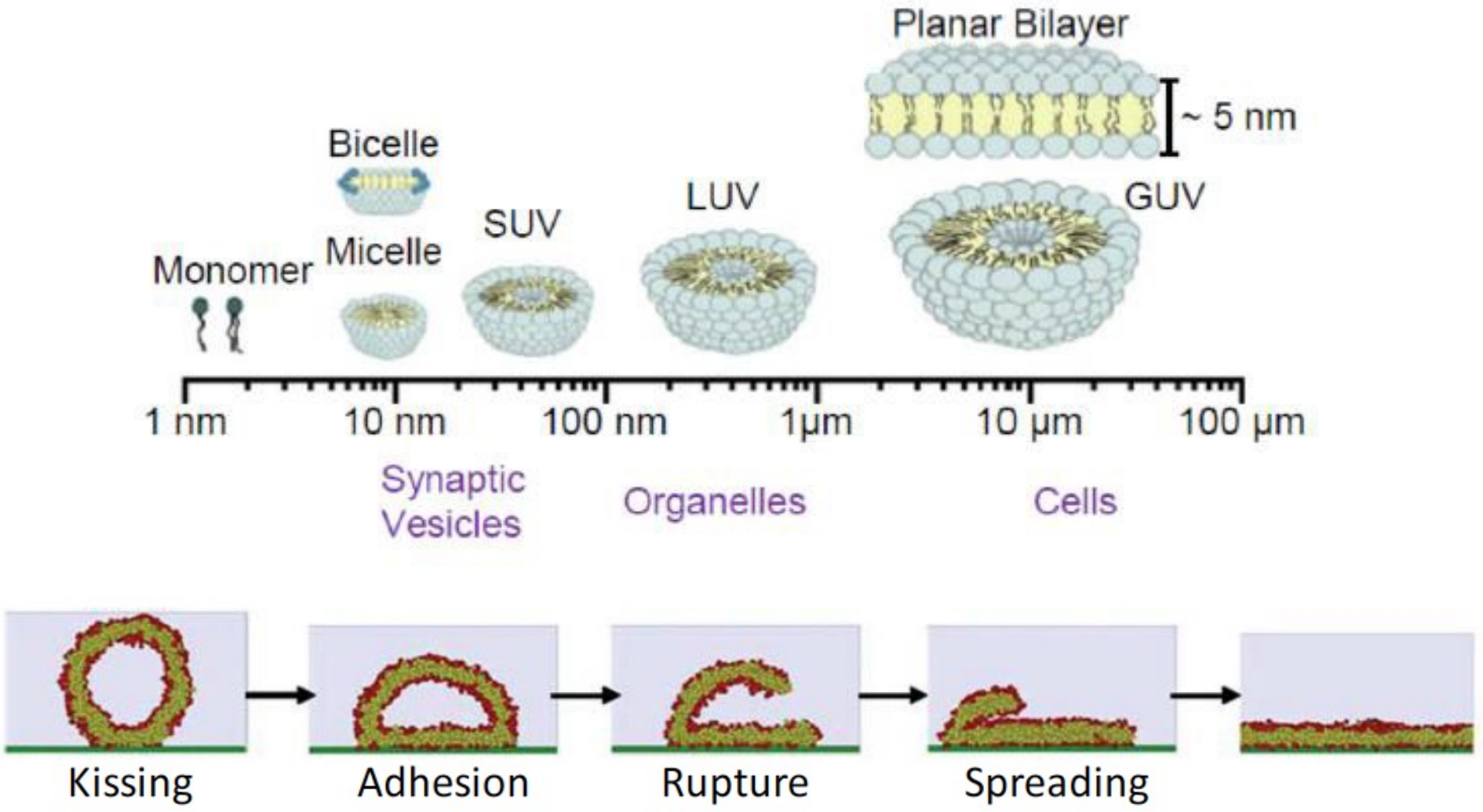

Cell membrane: an optimized 2D fluid system

Membrane fluidity depends on the type of lipid:

Saturated lipid are more ordered, therefore mode rigid then the **unsaturated** ones

Cholesterol is hydrophobic, but reacts with a OH^- group with the hydrophilic heads of neighbor phospholipids

Low T: chol is a spacer, fluidity high

High T: chol stabilizes the membrane (sealing)

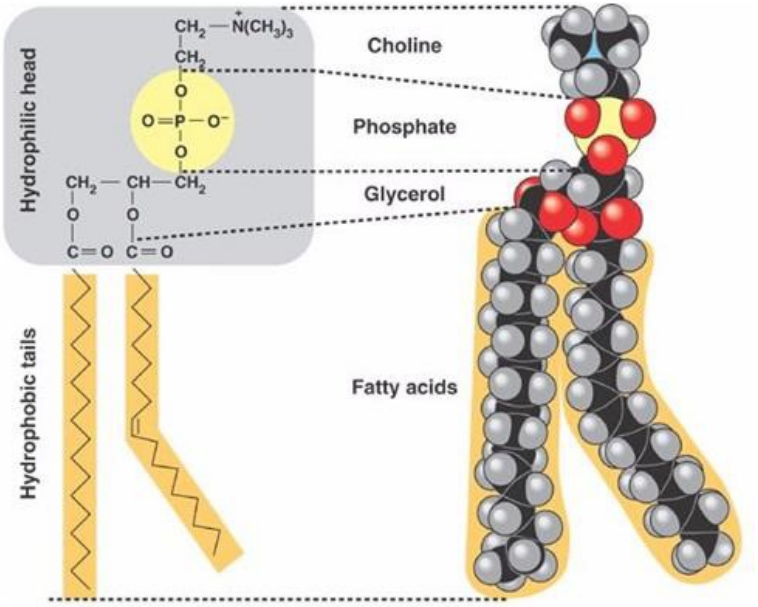

Stearic acid - saturated

Oleic acid - unsaturated

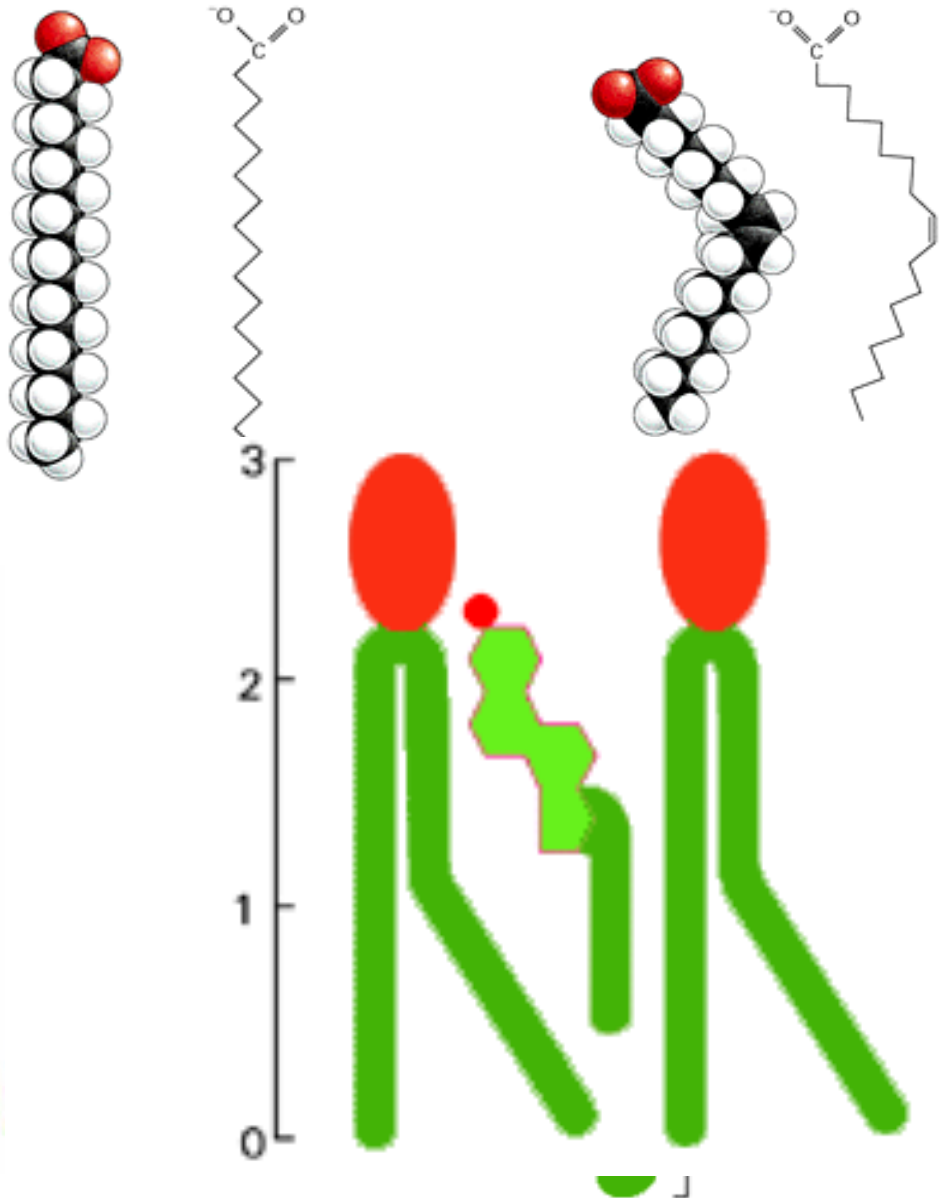

Study of unstructured protein oligomerization

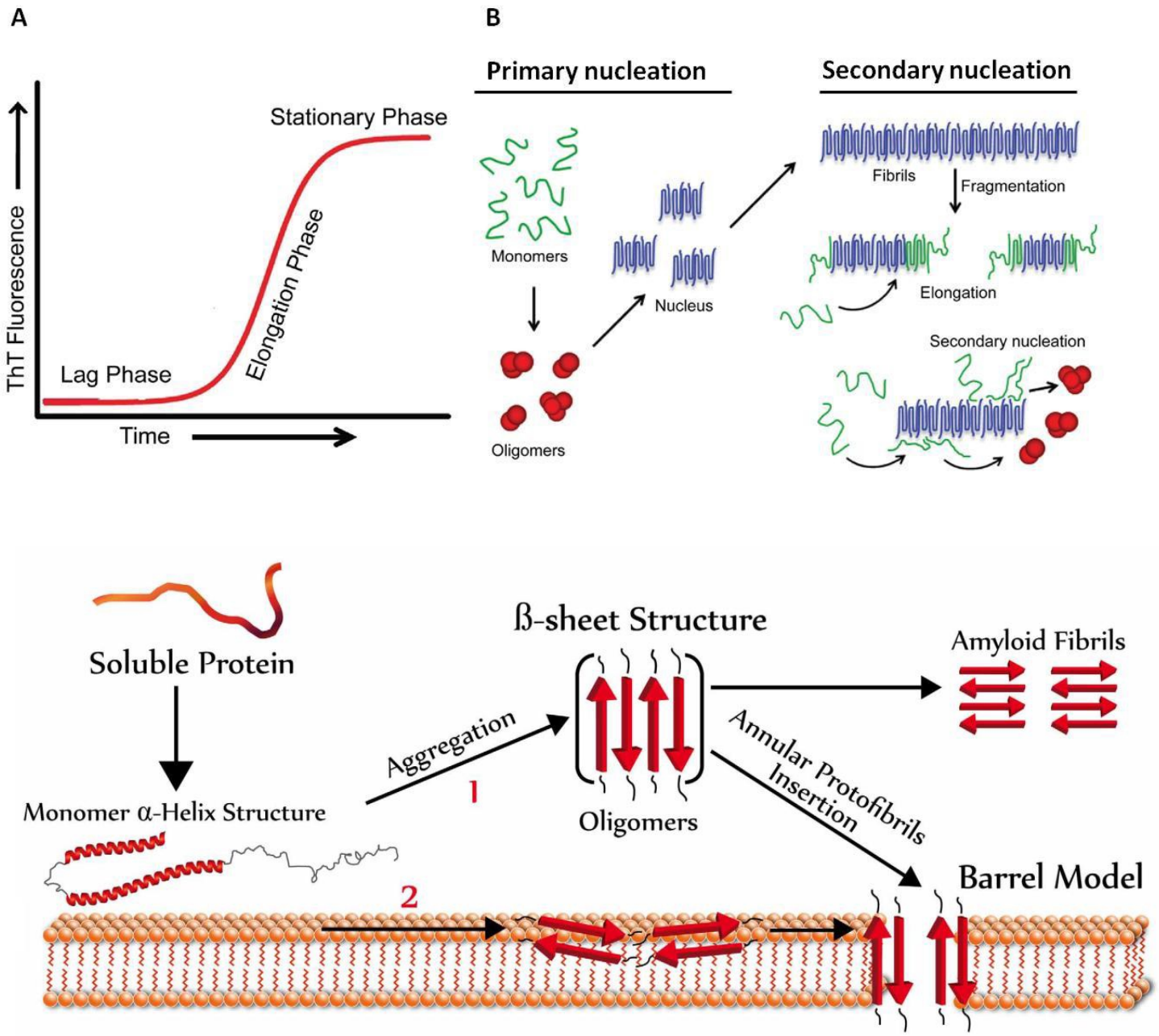

Multicomponent lipid membranes

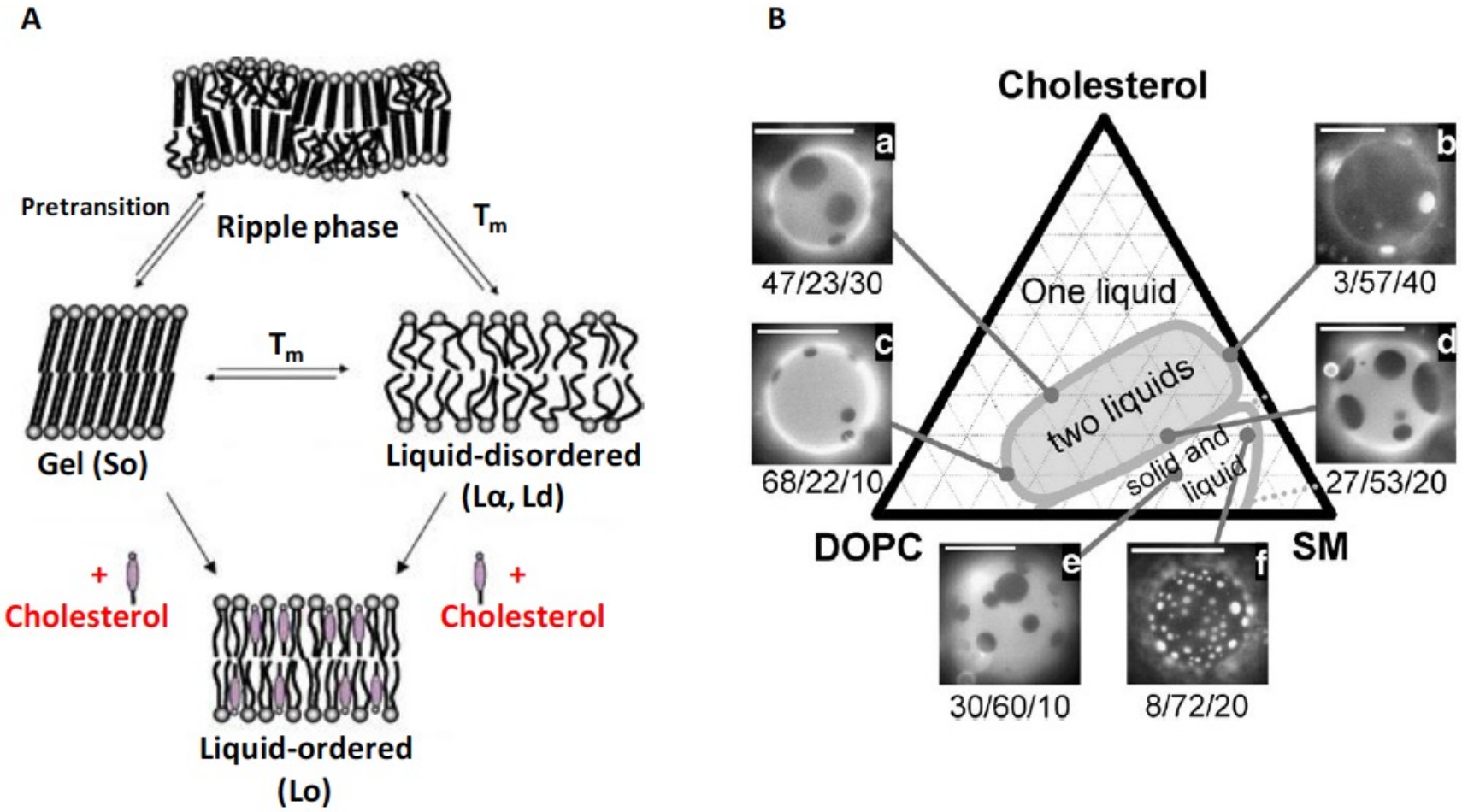

Model cell membranes-rafts

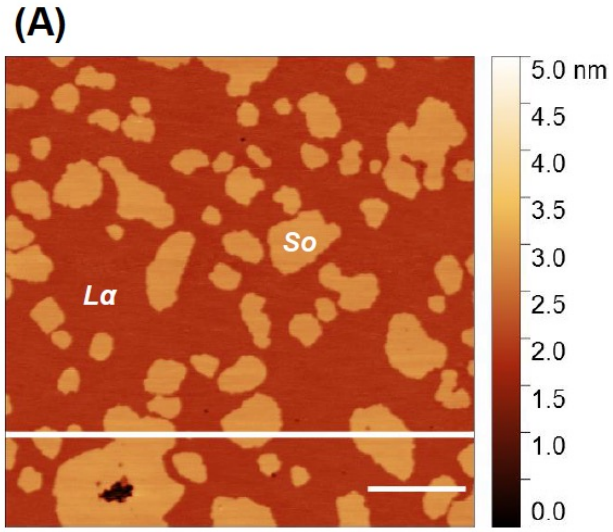

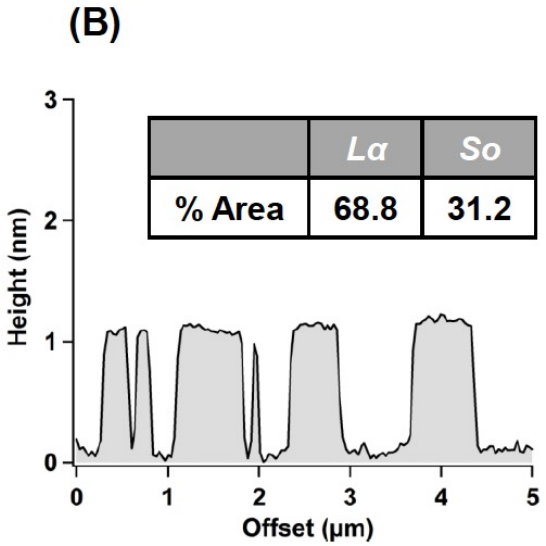

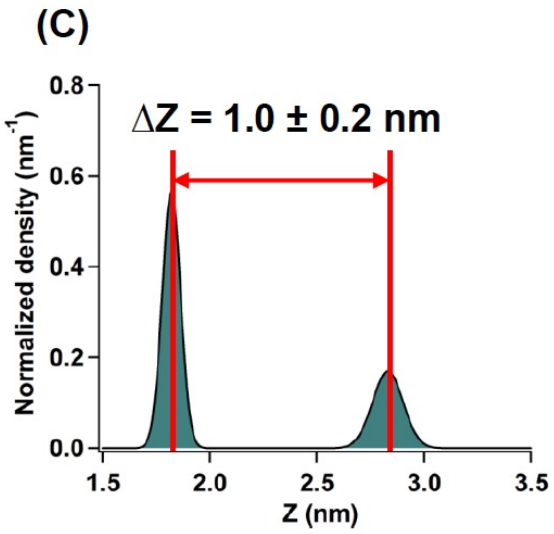

Coexistence of liquid-disordered (*Lα*) and solid-ordered (*So*) phase in planar supported lipid bilayer mimicking raft-like domains.

(A) AFM topography image of ternary SLB composed by DOPC, SM and cholesterol (66:33 +5% Chol). Image was taken in aqueous buffer in dynamic AC-mode. Scale bar: 1.0 μm. **(B)** Section analysis (white line in (A)) shows So-domains protruding from the fluid matrix (Lα) of SLB of ≈ 1.0 nm. **(C)** The height distribution graph

Model membranes-rafts

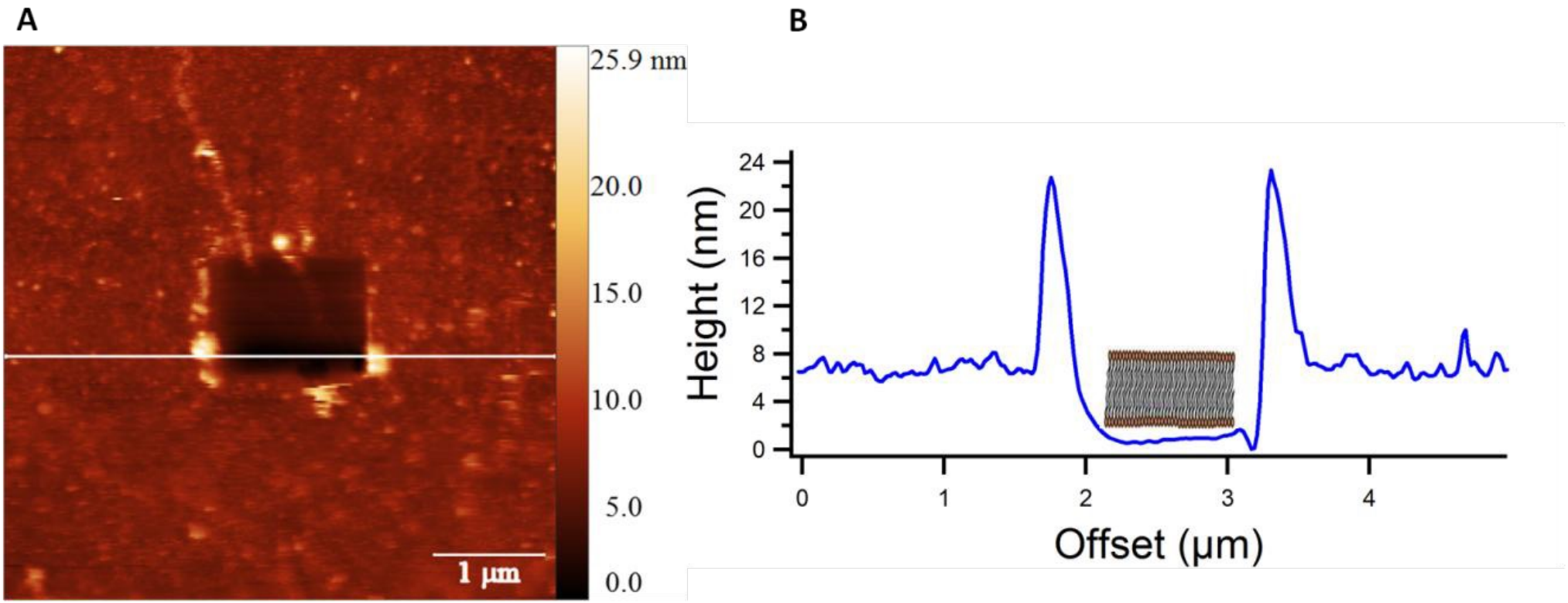

DOPC/SM (66:33)

A + 5 % Chol

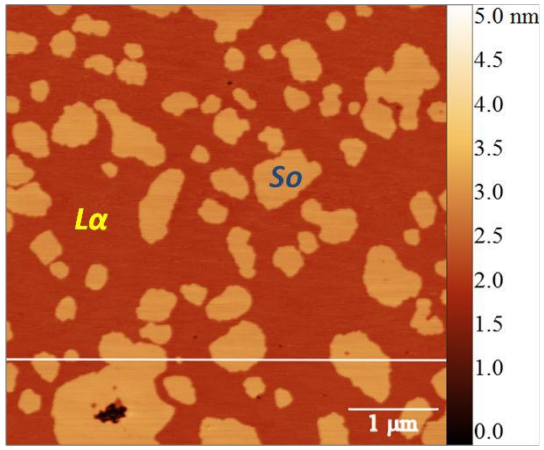

B + 20 % Chol

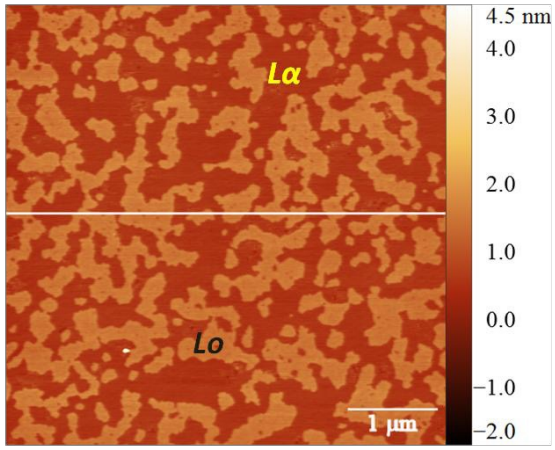

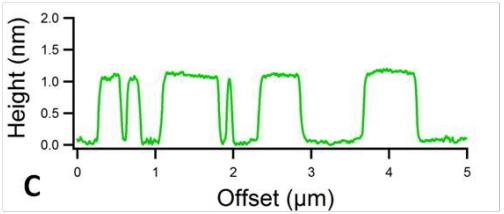

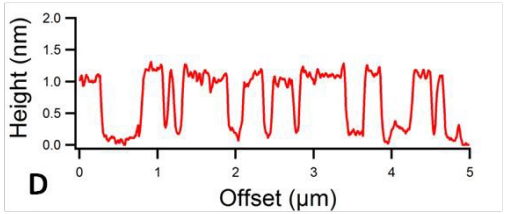

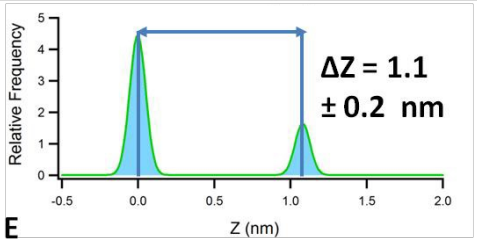

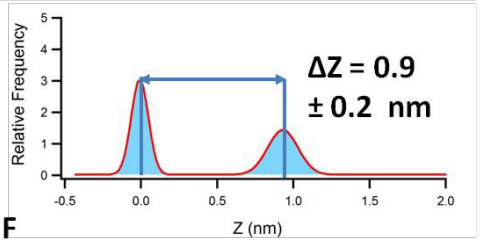

Lα	So
64.2 %	35.8 %

Lα	Lo
57.0 %	43.0 %

G

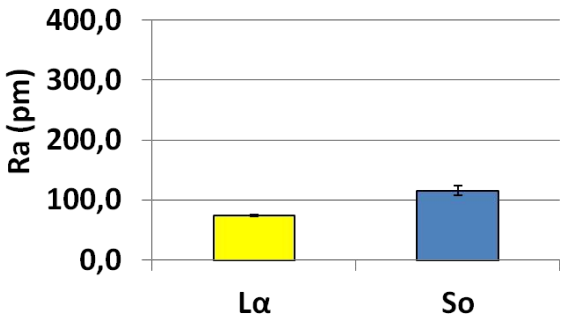

H

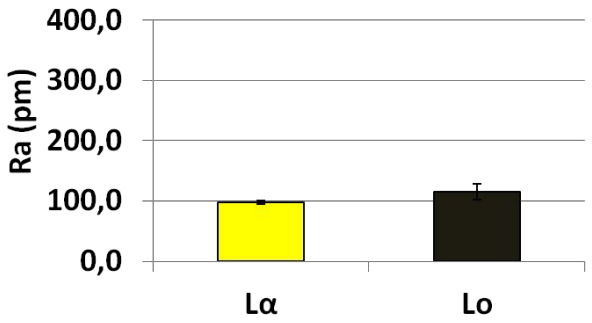

Membrane proteins

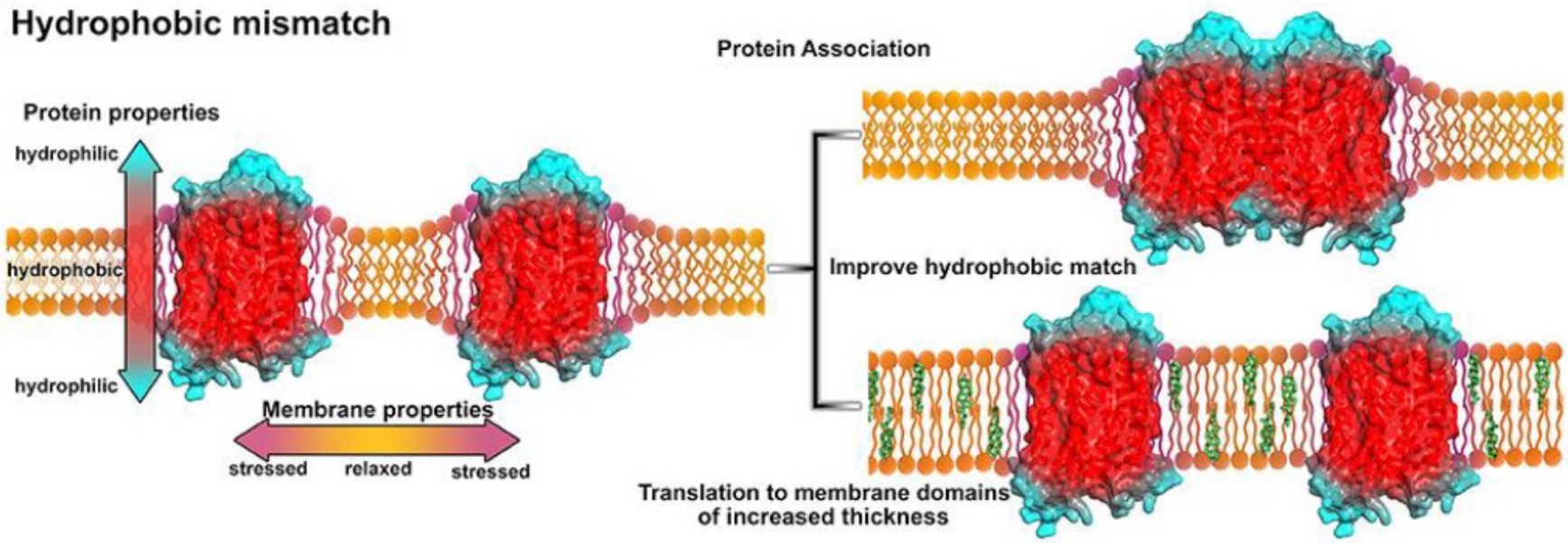

Lipid-protein interactions are very important for the stabilization of protein structure, regulation of protein activity and for partition of proteins in different lipid domains, as in lipid rafts. At the molecular level, these interactions drive the complex organization of plasma membrane.

Membrane proteins: Gangliosides

DOPC/SM (66:33) + 5 % Chol + 2.5 % GM1

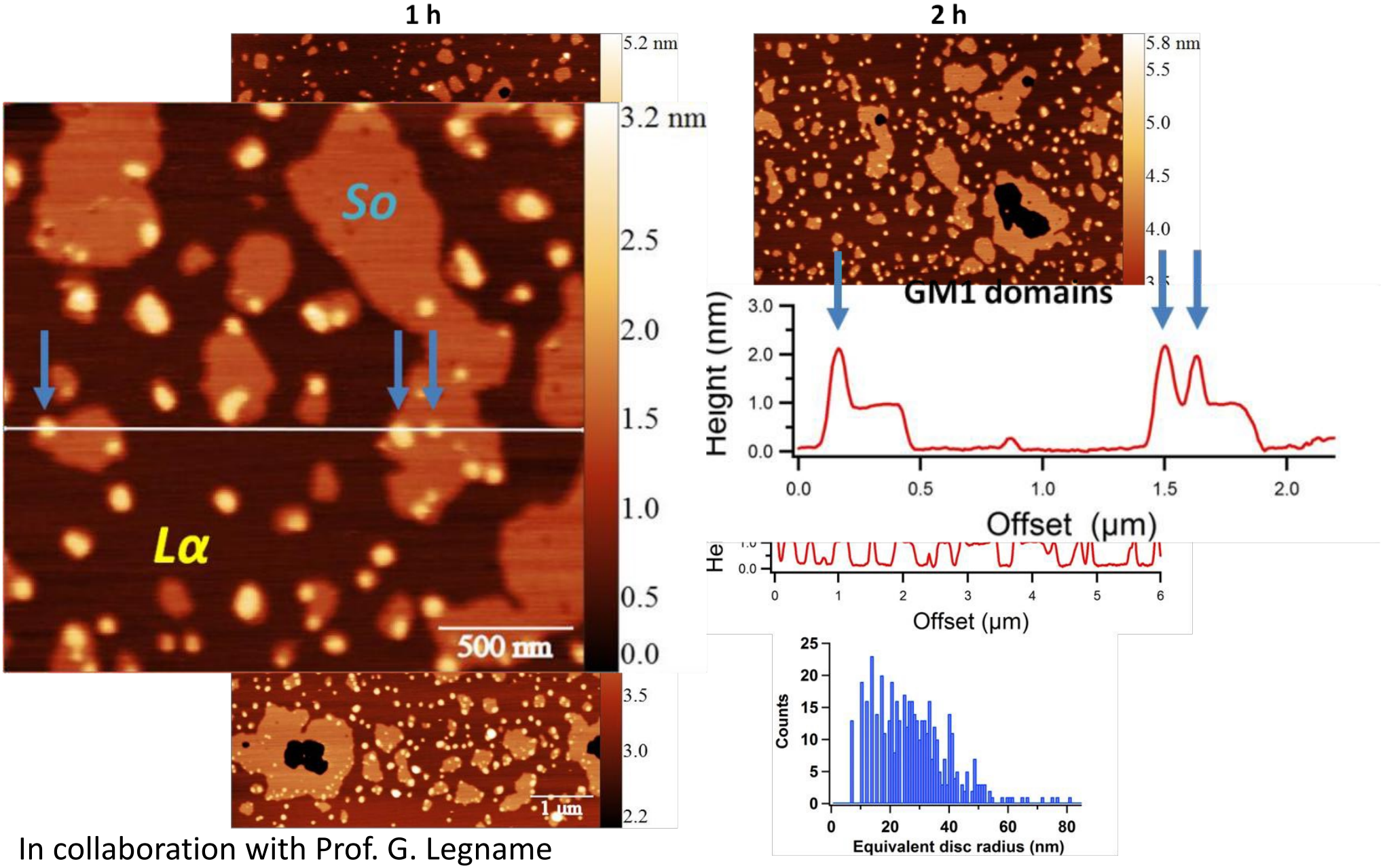

In collaboration with Prof. G. Legname

Membrane proteins: **Lipidated-Prion protein (PrPC)**

PrPC is a GPI-anchored protein that is predominatly localized in the outer leaflet of the neuronal cell membrane. Although the biological function of PrPC has not been fully understood yet, its membrane attachment via a GPI anchor seems to be critical for the conversion into the pathological PrPSc isoform, which generates highly insoluble, toxic aggregates.

DOPC/SM (66:33) + 5 % Chol + FL-PrP-MA (1 h)

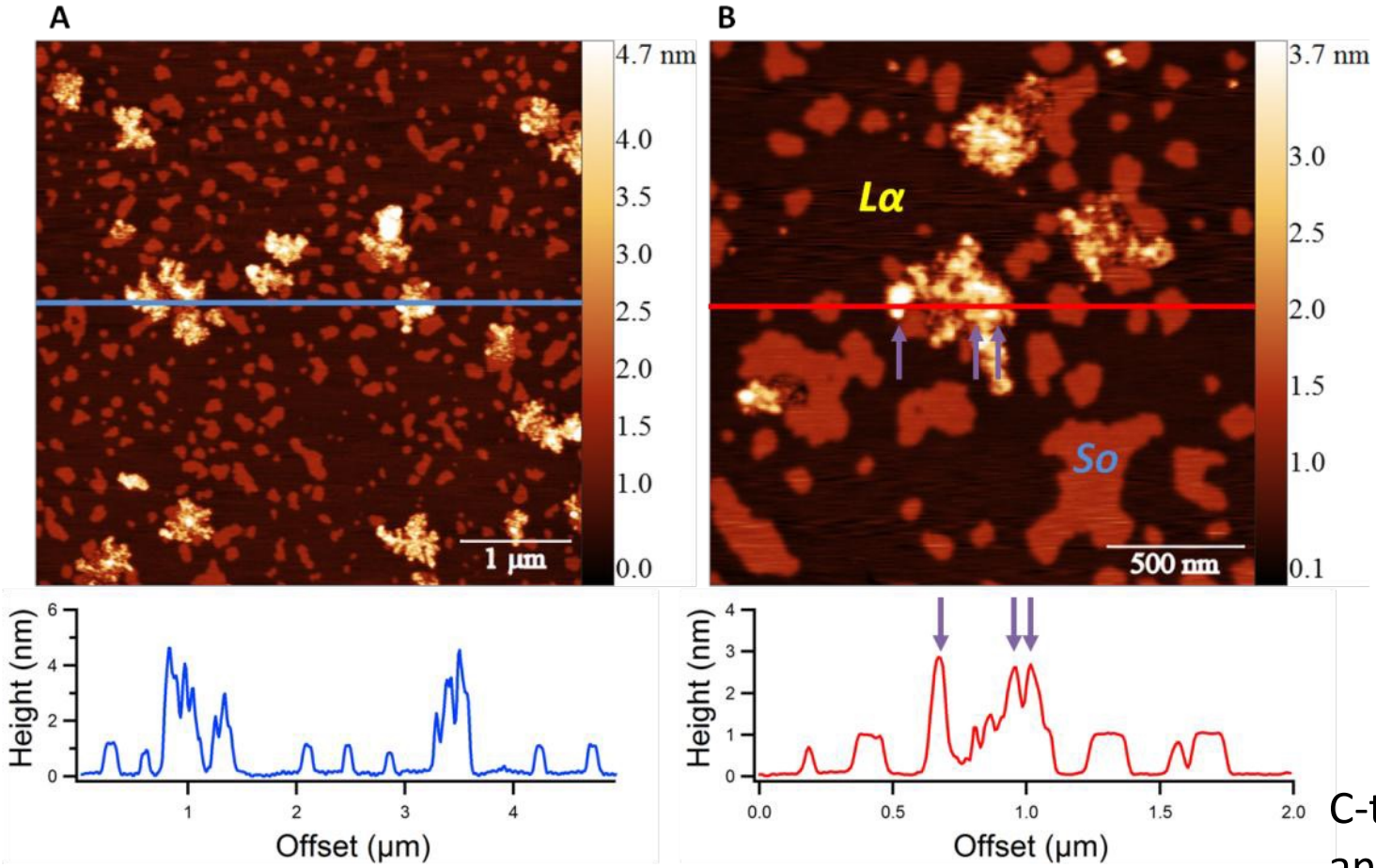

Several evidences support the idea that lipid environment has a key role in prion conversion and propagation, especially the association of PrPC with lipid raft domains

C-terminal membrane anchor (MA)

In collaboration with Prof. G. Legname

Membrane proteins: **Lipidated-Prion protein (PrPC)**

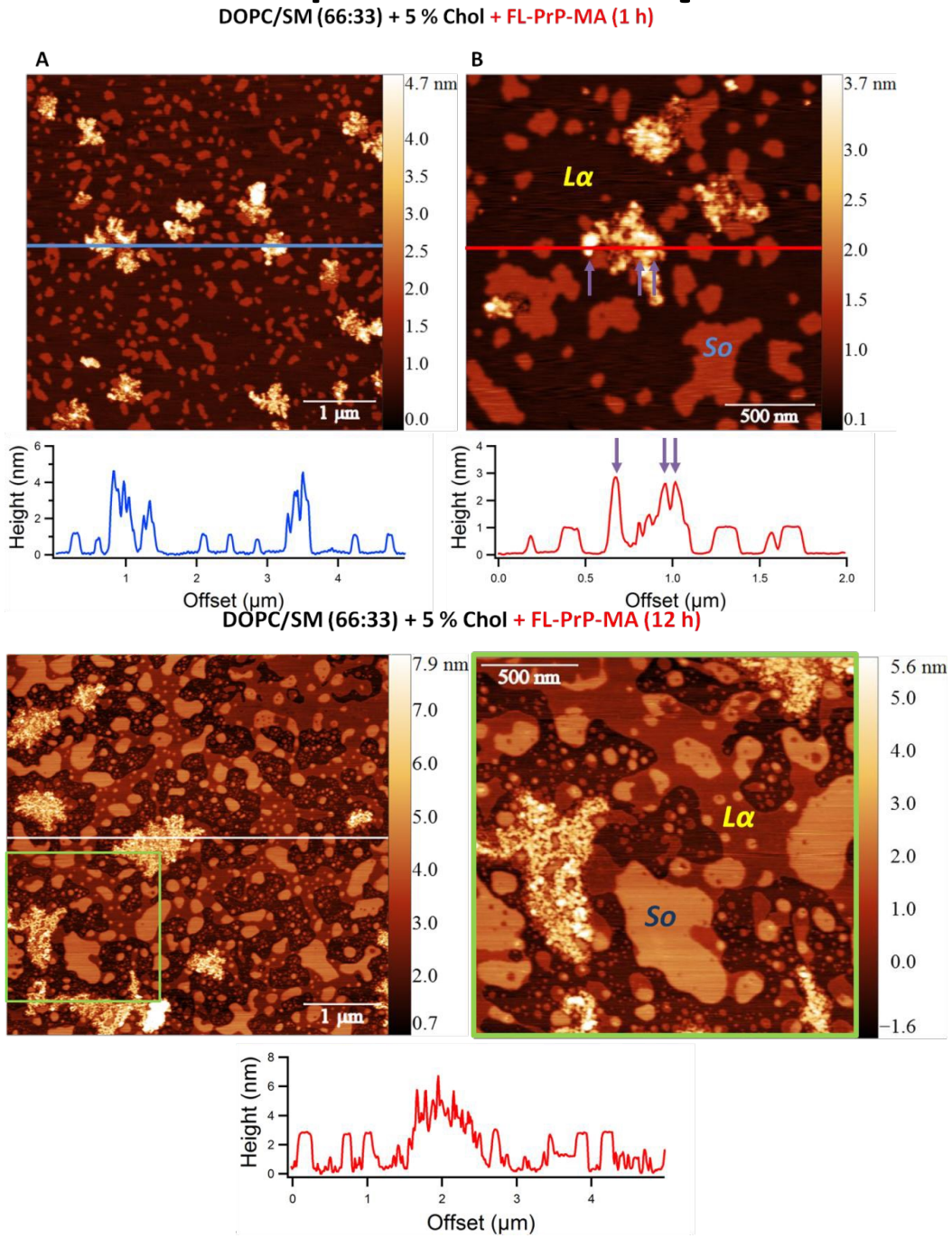

FL-PrPC-MA interacts with lipid raft domains without affecting the fluid phase of the bilayer. This could be due to the MA activity, which targets the protein to the ordered islands of membrane. However, formation of aggregated protein clusters which resemble oligomer accumulation are observed.

Membrane proteins: **Iron-mediated Alpha Synuclein (αS) aggregation**

Iron is implicated in the electron transfer during cellular respiration and as cofactor in the catalysis of enzymatic reactions.

Iron is potentially toxic when is present at high concentrations in the cell. It has been demonstrated that the total amount of iron increases physiologically in the brain with age and that this fact could be correlated with the old-age onset of PD

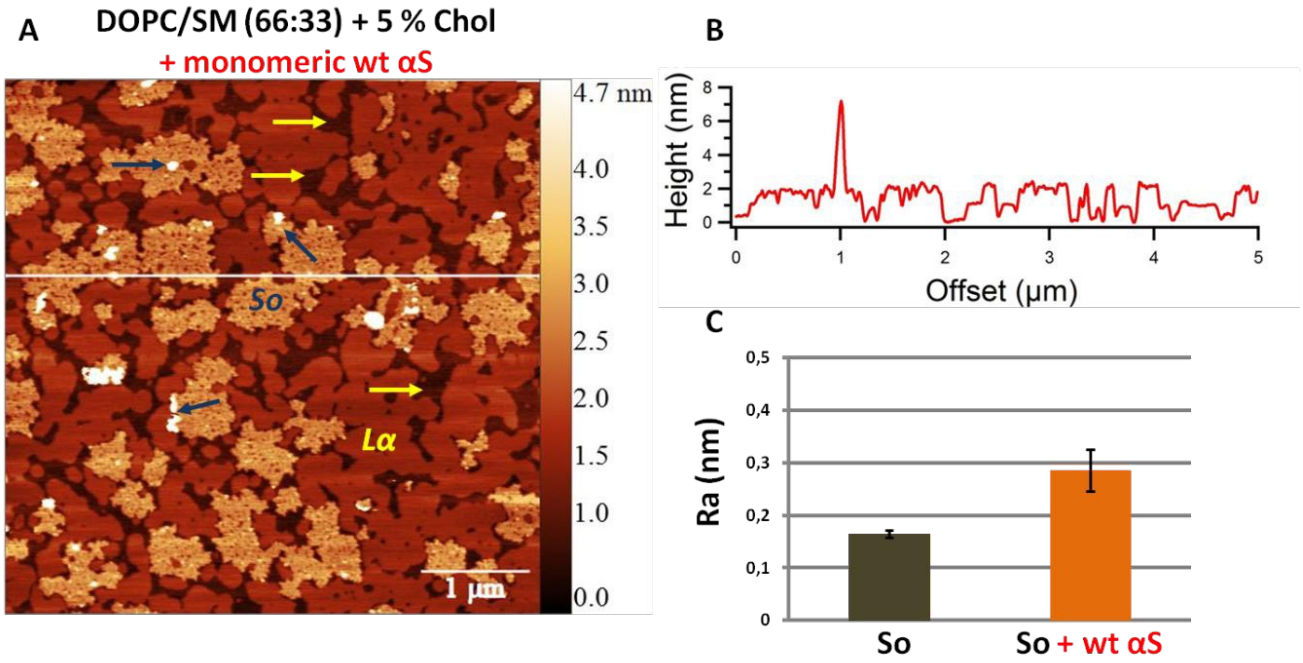

Membrane proteins: **Iron-mediated Alpha Synuclein (αS) aggregation**

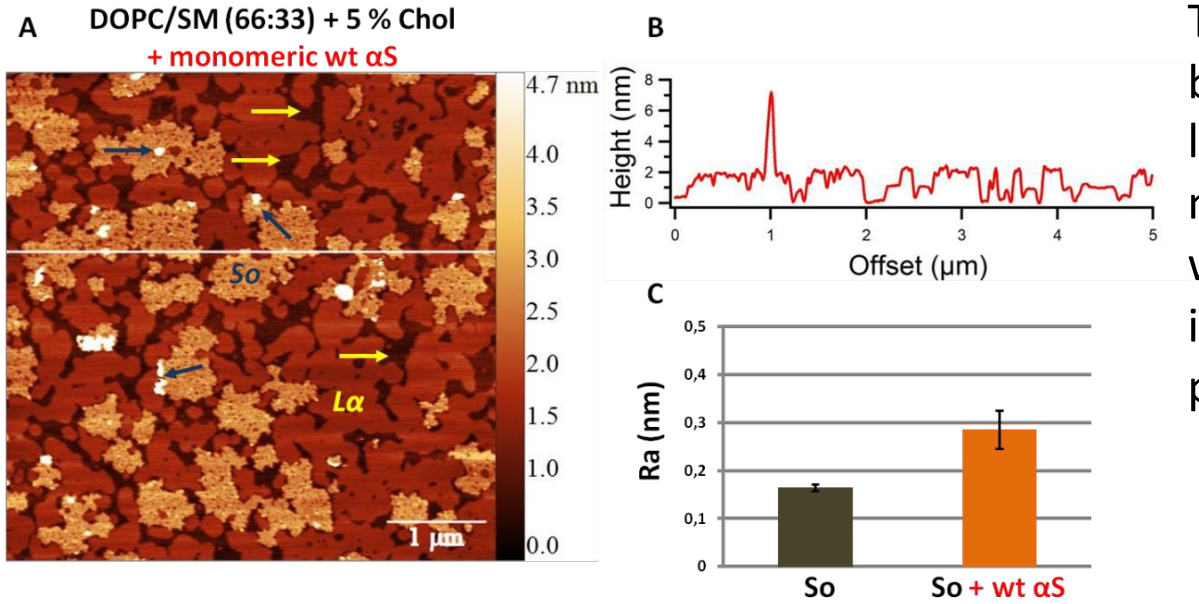

The wt αS seems to interact with both lipid phases (Lα and So) leading to a change in the morphology of raft-like domains which appear to have irregular and indented borders, as well as a more pronounced roughness.

A53T: mutant form of αS, responsible for an early stage familiar development of PD and more prone to aggregation
A53T seems to interact preferentially with the fluid lipid matrix causing damage sites without affecting the ordered domains

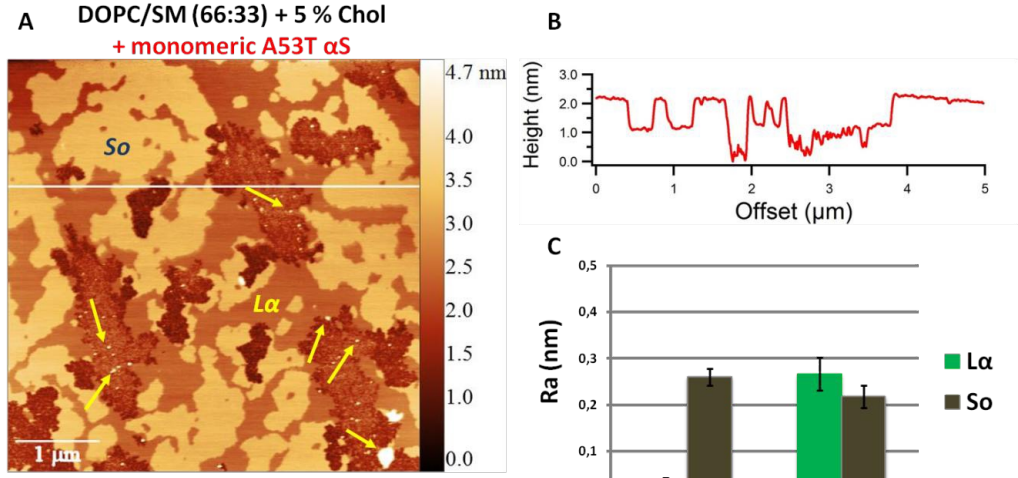

Lα	So	defect sites
29.3 %	32.2 %	38.5 %

Membrane proteins: **Iron-mediated Alpha Synuclein (αS) aggregation**

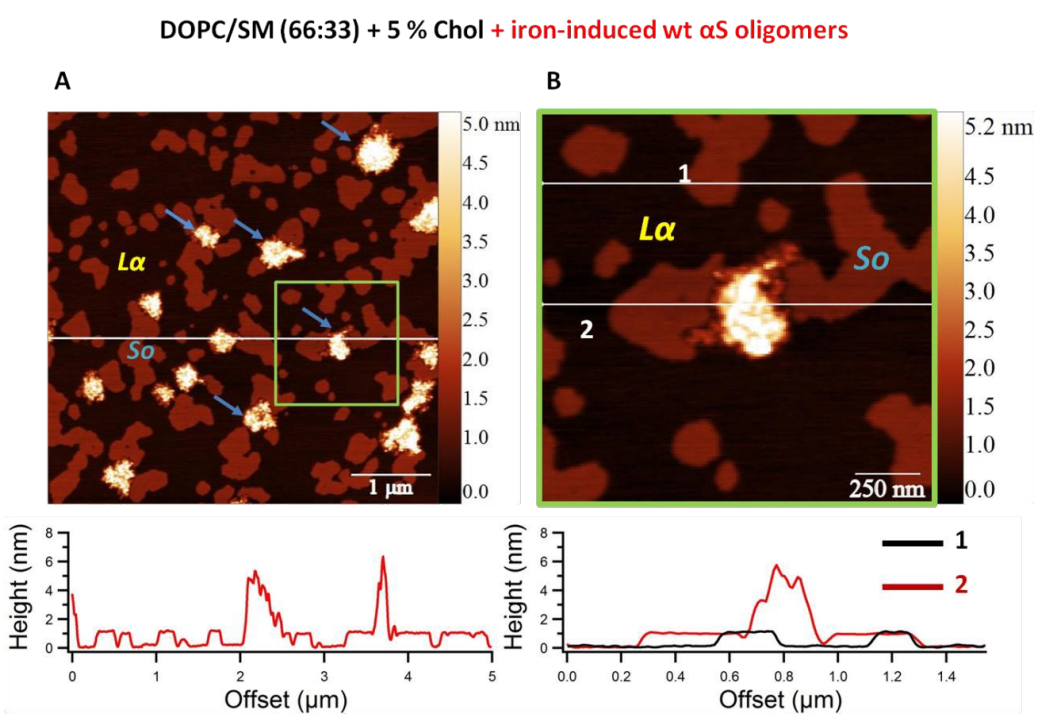

Iron-induced oligomers interaction with raft-like membranes revealed an accumulation of these misfolded structures on the ordered domains, forming protein clusters, for both wt and mutant A53T αS

The protein clusters of the mutant species are bigger in terms of dimensions and coverage of the membrane area, reflecting the faster rate of aggregation in the presence of iron compared to the wt αS

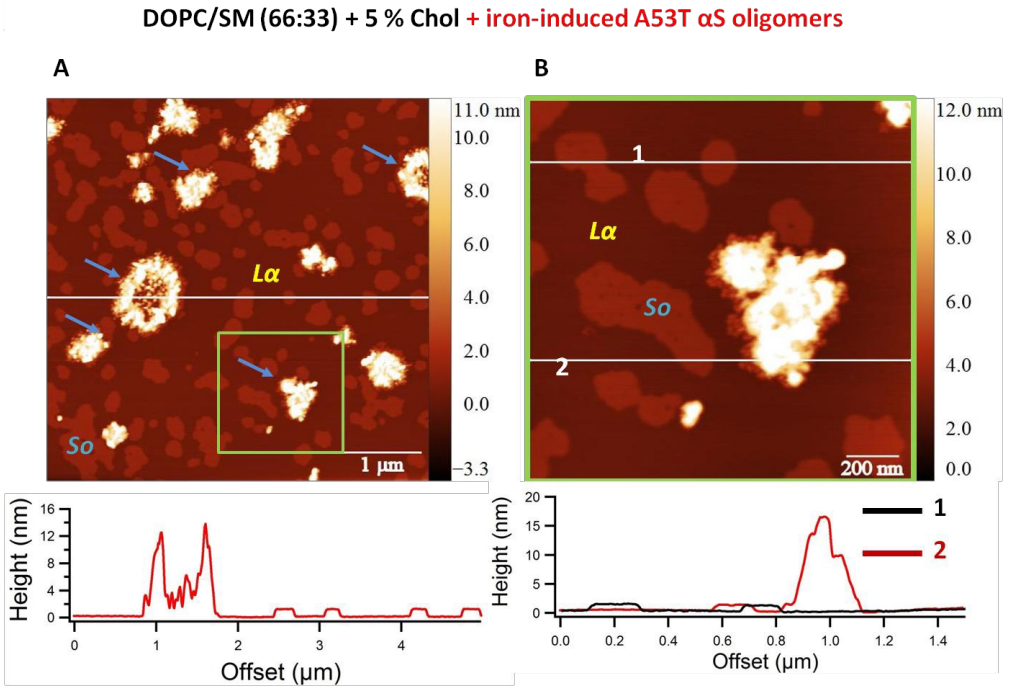

Purple membranes

Light activation of these proteins modulates cellular excitability with millisecond precision

The so-called **Purple Membranes (PM)** are part of the membrane of the archaea Halobacterium salinarium, an extremophile naturally found in salt saturated water.
This particular biological membrane **contains only one protein, bacteriorhodopsin (bR) and about seven different unusual membrane lipids** assembled in a hexagonal lattice of bR trimers (p3 crystallographic point group, 6.2 nm lattice constant).

C

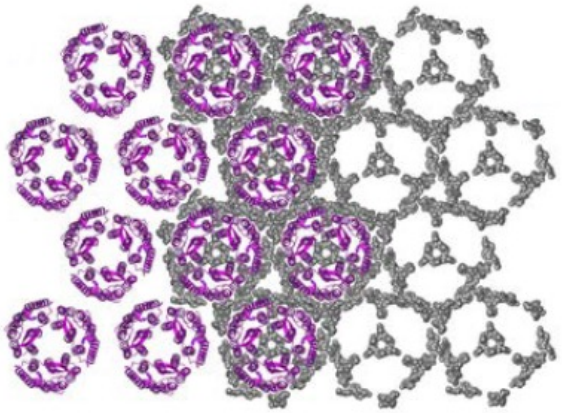

2D hexagonal lattice

The protein-lipid ratio has recently been determined to be **10 lipids per bR.**
The proteins represent 75% of PM mass and cover 50% of the membrane surface.
bR acts as a **light-driven vectorial proton pump** which converts photonic energy into a proton gradient across the membrane.
The induced electrochemical gradient is subsequently used by ATP-synthase as an alternative driving force to produce ATP in mediums particulary poor in oxygen.

The absorption spectrum of bR in its ground state (maximum absorbtion at 565 nm) is responsible for the purple colour of PM

B

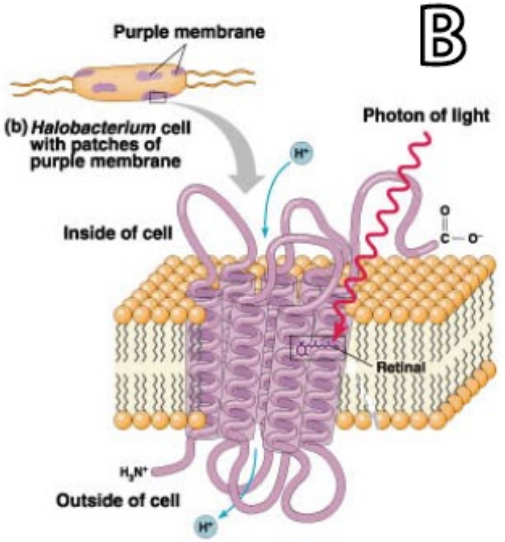

Purple membranes

PM is one of the best known biological membrane and an important model system to confront new theories and experimental methods.
bR was indeed the first integral membrane protein which structure was determined by X-ray crystallography of three-dimensional crystals grown in cubic lipid phase (non soluble proteins: difficulty in crystallization!)

N.B: membrane proteins are either peripheral (at the surface) and soluble in high ionic strenght acqueous solution (1 M salt) or integral, and can be solubilized only with detergent

All the protein membranes are coded by 20-30 % of the genome! But of all the known protein structures, only 5 % is of membrane proteins!

Purple membranes

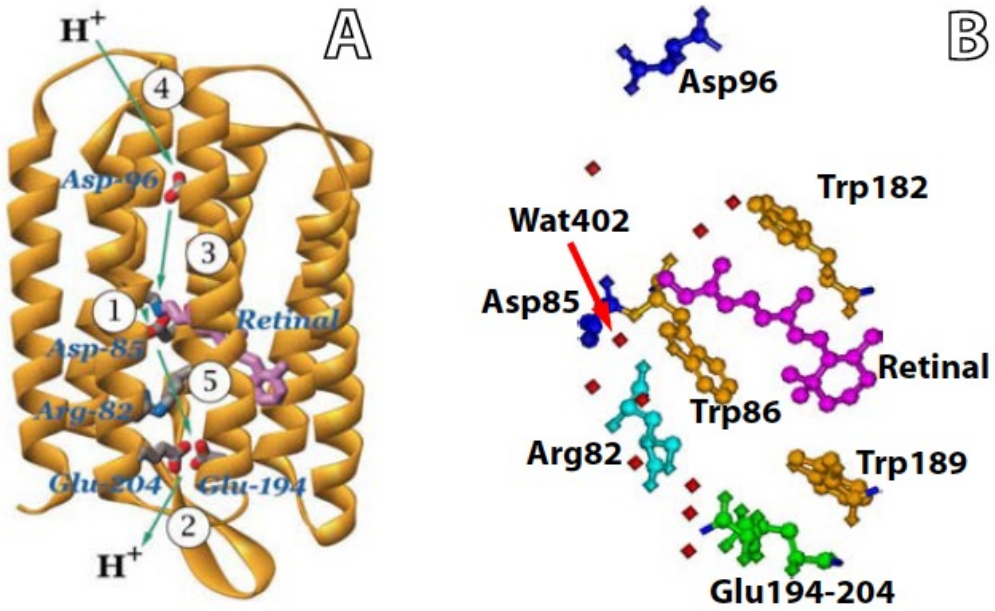

bR is an integral 26 KDa membrane protein composed 248 amino acids arranged in 7 transmembrane α-helices that surround a central cavity which encloses a chromophore, the retinal, linked to the protein backbone (Lys216 residue, helix G) via a Schiff base.

When the protein is in its fundamental/ground state (called bR state), the retinal chromophore adopts an all-trans configuration. Upon light absorption by the protein, the retinal can isomerize around its $C_{13} = C_{14}$ double bond, adopting a 13-cis configuration. This new chromophore conformation triggers a series of structural rearrangements in bR leading to the pumping of a proton from the inside to the outside of the archea.

Purple membranes

In PM, **bR molecules lateral and rotational movements are prevented by the crystalline assembly**. PM is rather rigid with a viscosity typically 10^3-10^4 higher than that of halobacterial membrane lipids.

Within one trimer, the proximity between the bR molecules allows direct protein-protein interactions through the formation of salt bridges, hydrogen bonds and van der Waals interactions between the α-helices of the different proteins involved.

These interactions are however not sufficient to explain the important trimer stability in which specific protein-lipid interactions are involved. The exceptional cohesion within a single trimer is believed to be related to the protein activity through cooperativity.

Purple membranes

The isomerization of the retinal chromophore modify temporarily the position of charged residues within the protein allowing directional pumping of one proton over a **~ 10-20 ms photo-cycle**. The modifications of the retinal local electrical environment can be observed spectroscopically

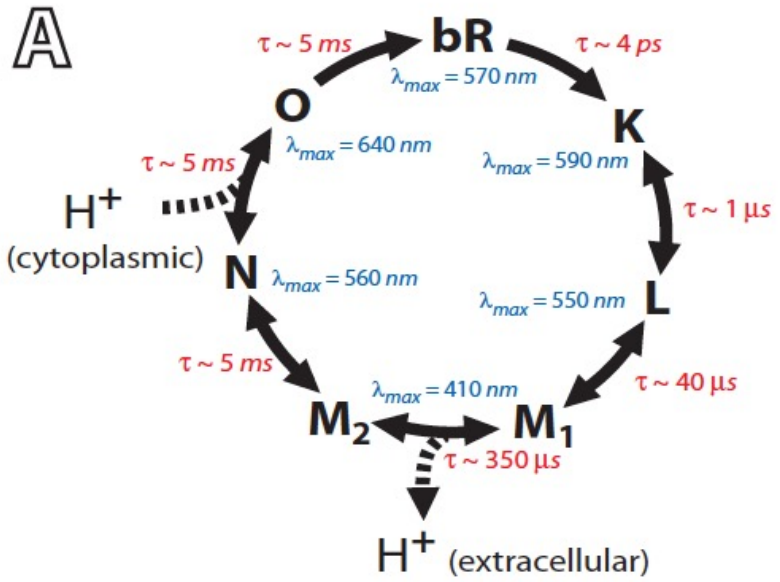

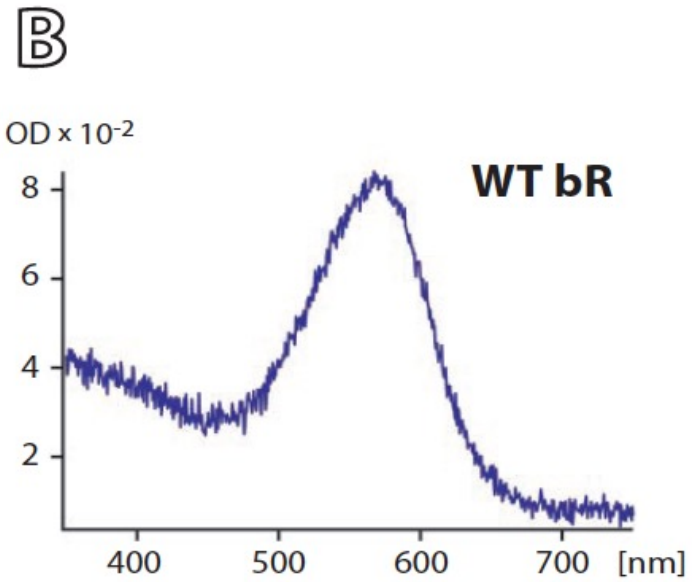

Purple membranes

PM contains many different lipids some of which are not found in any other membrane and are necessary for bR activity, also in reconstituted membranes. To date, seven different lipids have been reported :
three phospholipds, two glycolipids, squalene and traces of vitamin MK8.

The requirement of a fixed membrane composition indicates that **selective interactions occur between bR and certain lipid molecules** and that these interactions are essential for lattice assembly and bR function.

Phospholipids represent ~ 40% of PM lipids. their head-group comports two negative charges which makes them particularly hydrophilic. Fluorescence studies have demonstrated that phospholipids are located mainly in PM cytoplasmic leaflet inter-trimer space.

Glycolipids represent ~ 30% of PM lipids. Unlike phospholipids, glycolipids show clear patterns in PM diffraction experiments suggesting that they are specifically and tightly bound to bR.

Purple membranes

Local probe techniques have also been used to study purple membrane (Tamayo et al. 1995) and bR was **the first membrane protein extensively studied by atomic force microscopy and force spectroscopy.**

The analogy between bR and **GPCR (G-protein** (mol. Switches) **coupled receptors)** is also an important factor contributing to the use of bR as a model system.

Unlike most of the prokaryotic α-helical membrane proteins which are composed of six or twelve transmembrane helices, **eukaryotic α-helical membrane proteins show a preference for seven transmembrane α-helices mainly because of the GPCRs**. The bR structure with seven transmembrane α-helices enclosing the active group is a characteristic of GPCRs. The first GPCR structure resolved, **bovine rhodopsin**, was achieved only recently and most of the previous pharmaceutical studies aiming at GPCR were based on the structure of bR. To date, the only GPCR structure resolved remains rhodopsin, a representant of the largest GPCR sub-family (A-family with 90% of GPCRs). Despite the fact that bR is not a GPCR, it is related to rhodopsins and remain an important model for pharmacological studies.

HR-AFM in membrane biology

High-resolution AFM has been applied to the imaging of bacterial membrane proteins, deriving the free energy landscape for domains within single protein mole

AFM

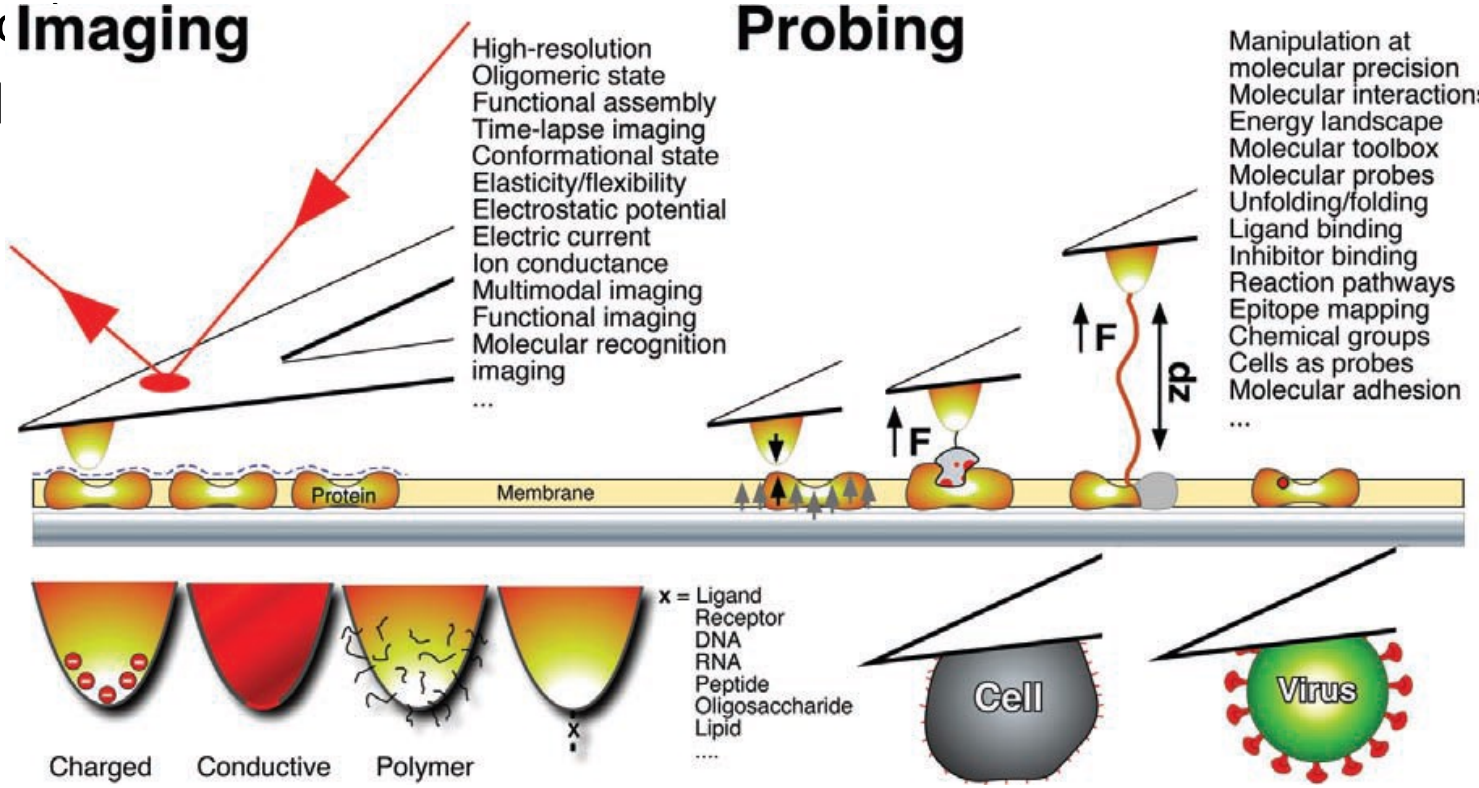

Imaging resolution in cell membranes: 10 nm
Imaging resolution in supported cell membranes: better than 1 nm (no fixing, labeling, Staining, room T, buffer solution)

S. Scheuring, D. Muller, H. Stalhberg, H.-A. Engel, A. Engel, *Eur. Biophys. J.* **31**, 172 (2002)

D.J. Muller et al. J. Mol. Biol. **(1999)** 285**, 1903-1909**

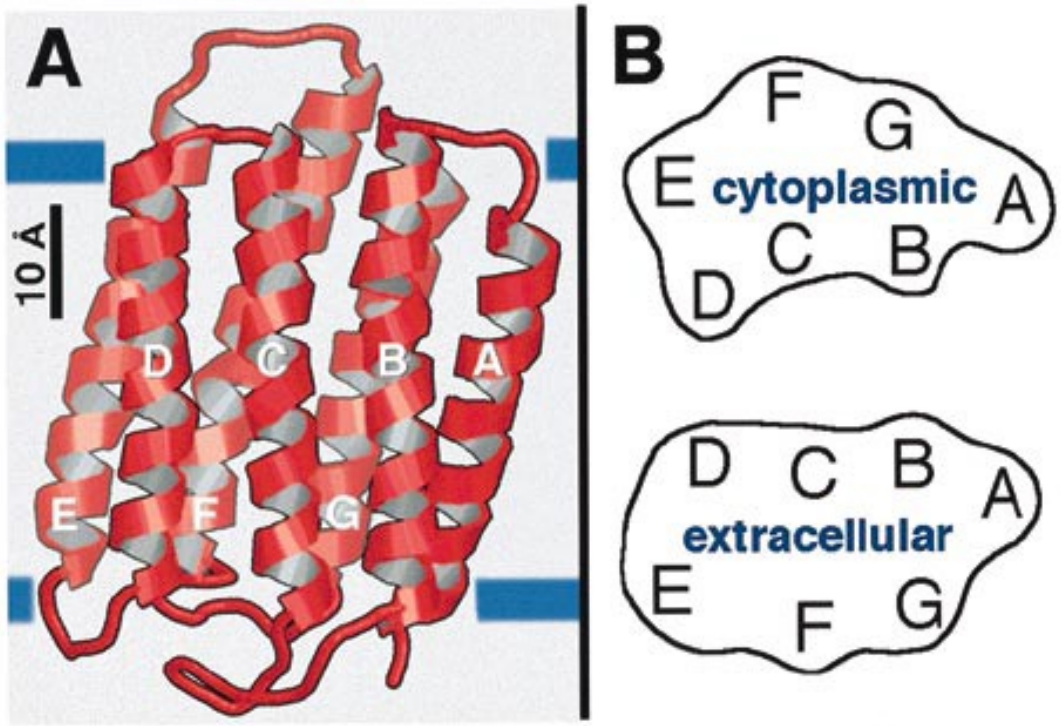

Structure of bacteriorhodopsin. (a) Ribbon representation as revealed by electron crystallography (Grigorieff et al., 1996). Because of their disordering, the N terminus of helix A and the C terminus of helix G were not resolved and the B-C loop was only partly resolved. Blue lines indicate the cytoplasmic and extracellular surfaces determined by Kimura et al. (1997).
(b) Outlines of 10 AÊ thick slices of the cytoplasmic and the extracellular BR surface.

D.J. Muller et al. / Biochimica et Biophysica Acta 1460 (2000) 27-38

PM reconstructed membrane on mica. Cytoplasmic vs. extracellular side

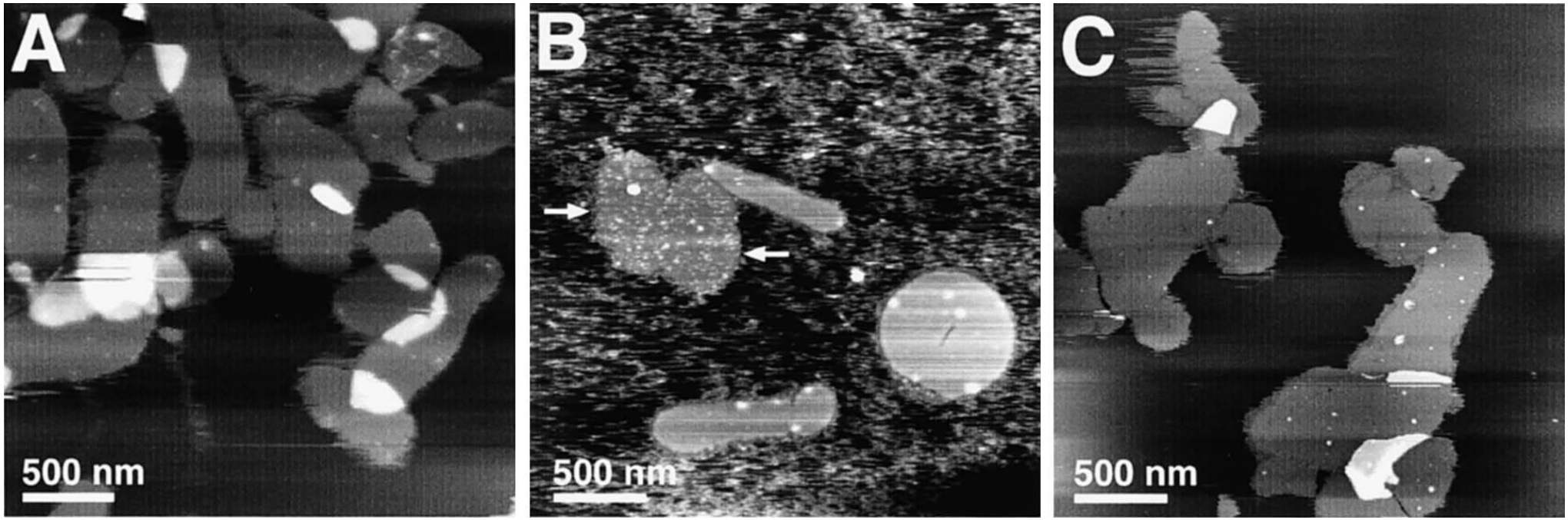

D.J. Muller et al. J. Mol. Biol. **(1999)** 285**, 1903-1909**

8.3(±1.9) Å **(**n . **398)**

6.4(±1.2) Å **(**n . **398)**

a=b=6.2±0.2 nm

The loops connecting the **alpha** -helices appeared to be disordered as they could not be resolved reliably.

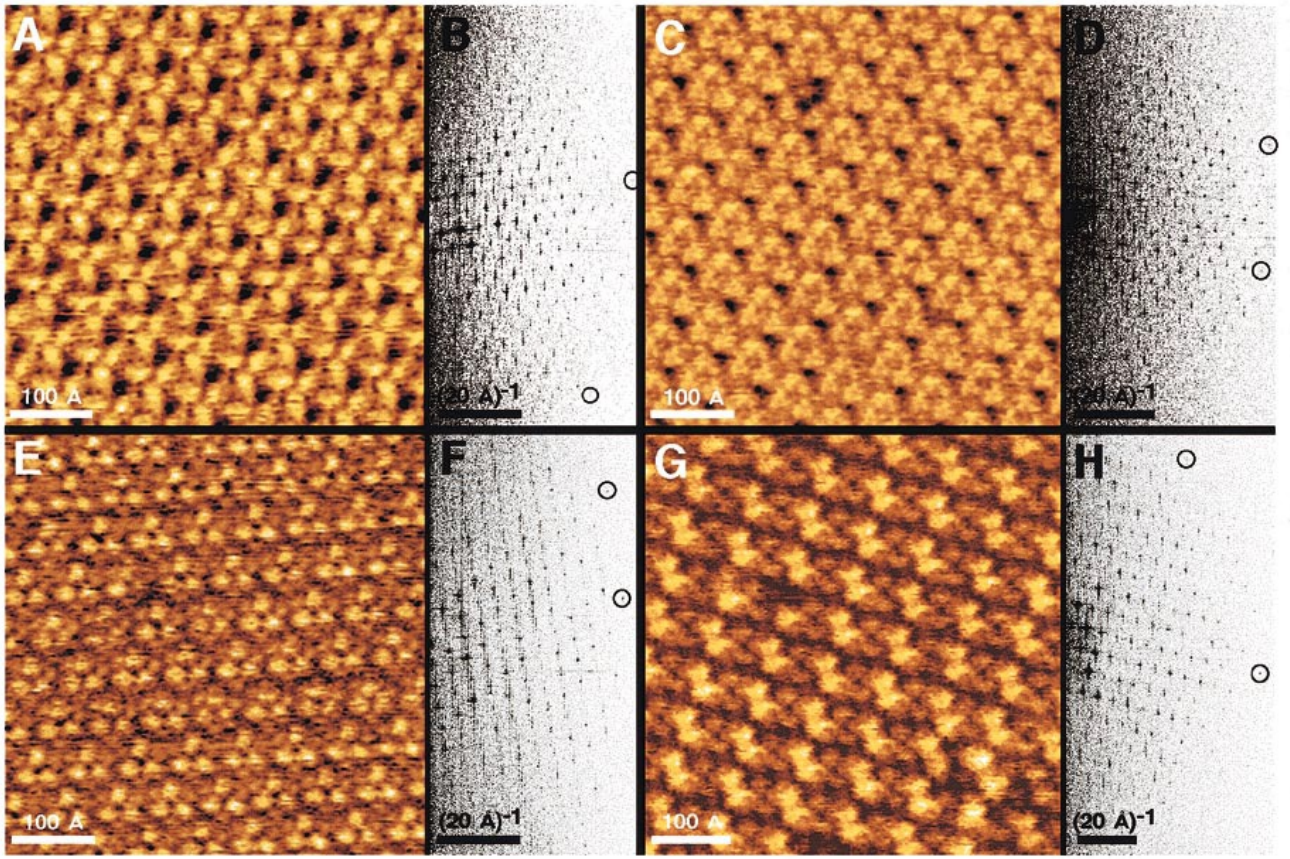

5.3(±0.7) Å **(**n . **320)**

in A protrusion arises from the loop connecting transmembrane **a** -helices E and F

(a) Native cytoplasmic surface recorded at 100 pN. (b) Power spectrum of (a). (c) Cytoplasmic surface recorded at 200 pN. (d). Power spectrum of (c). (e) Native extracellular surface recorded at 100 pN. (f) Power spectrum of (e). (g) Orthorhombic crystal of BR recorded at 100 pN. In this crystal form (p22121) the rows of BR dimers alternate, to expose either their cytoplasmic or their extracellular surfaces to the aqueous solution. (h) Power spectrum of (g).

N.B.: For the achievement of high resolution imaging a specific ionic concentration was required in order to balance van der Waals attractive forces with Electrostatic Double Layer repulsive forces (Muller & Engel 1997; Muller et al. 1999a).

D.J. Muller et al. J. Mol. Biol. **(1999)** 285**, 1903-1909 / Biochimica et Biophysica Acta 1460 (2000) 27-38**

Imaging of a statistically significant number of single proteins by AFM allows structural variability assessment and multivariate statistical classification to unravel the principal modes of the protein motion

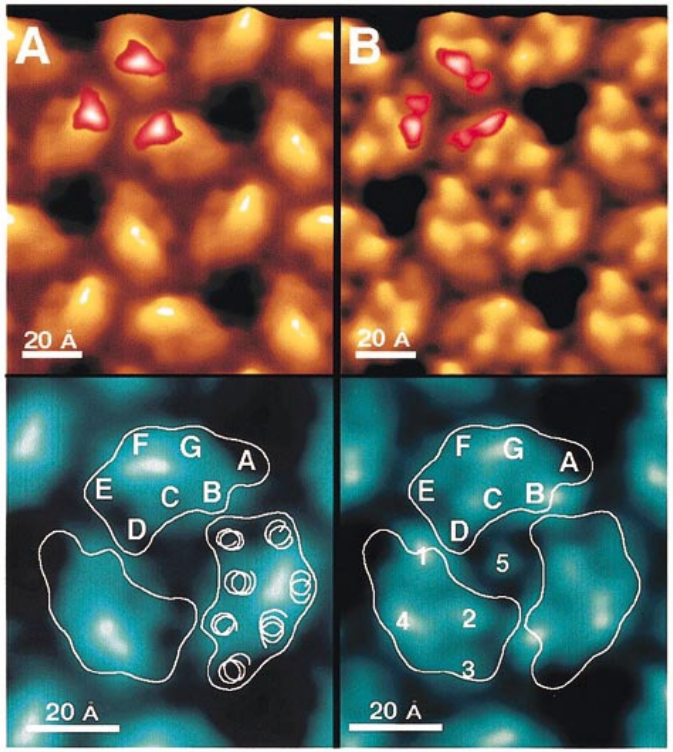

(C) Averaged extracellular surface of the bR trimer (average of 320 unit cells). The correlation average is displayed in perspective view (top, shaded in yellow brown) and in top view (bottom, in blue) with a vertical brightness range of 1 nm and exhibited a 6.1% root-mean-square (RMS) deviation from three-fold symmetry. To assess the flexibility of the different structures, standard deviation (S.D.) maps are calculated
(D) and had a range from 0.07 (lipid) to 0.12 nm (region of the FG loop).

D.J. Muller et al. J. Mol. Biol. **(1999)** 285**, 1903-1909**

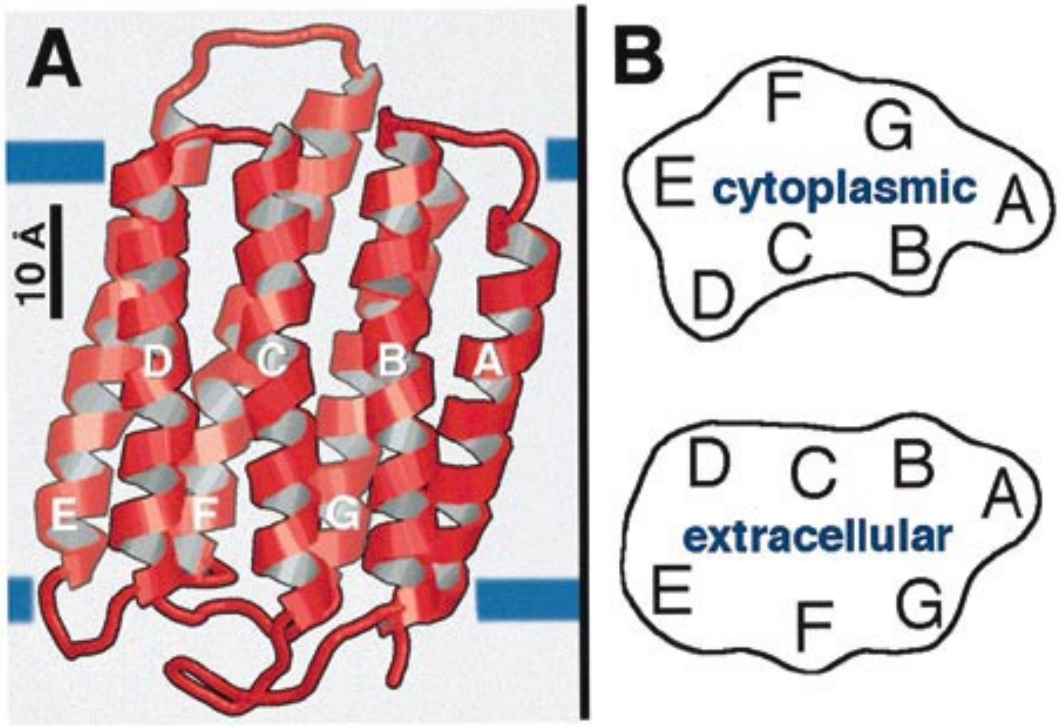

Structure of bacteriorhodopsin. (a) Ribbon representation as revealed by electron crystallography (Grigorieff et al., 1996). Because of their disordering, the N terminus of helix A and the C terminus of helix G were not resolved and the B-C loop was only partly resolved. Blue lines indicate the cytoplasmic and extracellular surfaces determined by Kimura et al. (1997).
(b) Outlines of 10 AÊ thick slices of the cytoplasmic and the extracellular BR surface.

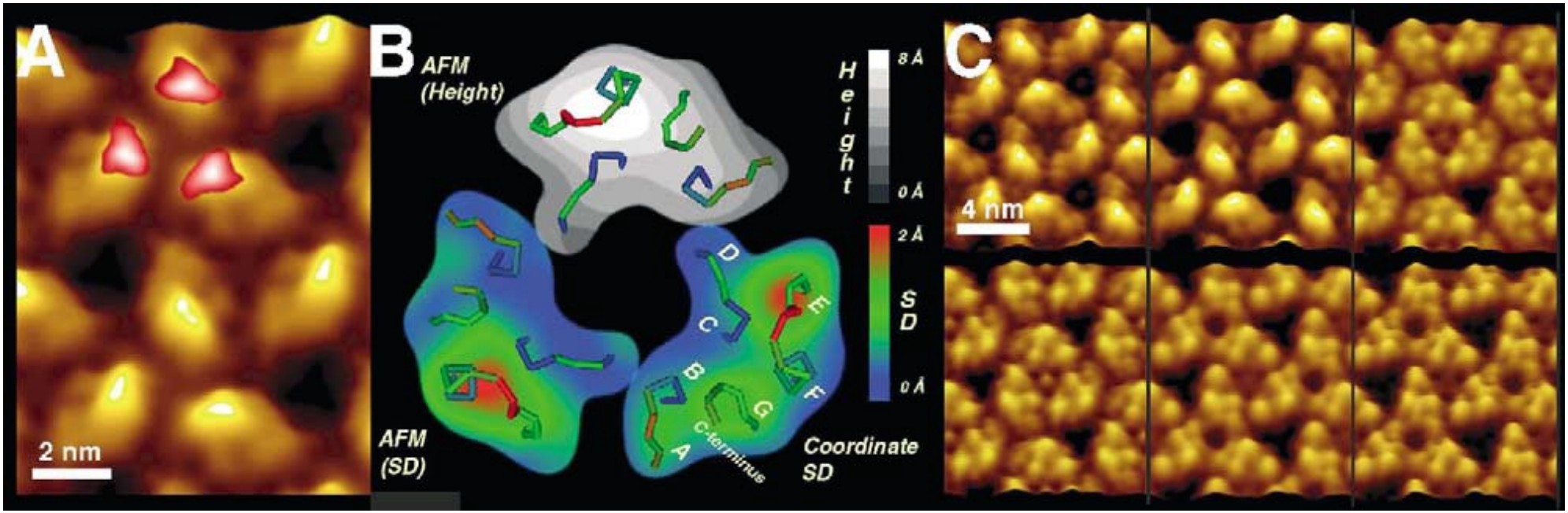

Fig. 16. Quantitative analysis of the native cytoplasmic purple membrane surface. (A) Correlation average of the AFM topograph recorded at an applied force of 100 pN (Müller et al., 1999b). Regions with enhanced flexibility are derived from SD maps and superimposed in red to white shades. (B) Different surface properties of bacteriorhodopsin. The surface loops are shown as backbone tracings colored according to the backbone coordinate root-mean-square deviation (SD) calculated after merging five different atomic models of bacteriorhodopsin (Heymann et al., 1999). The gray scale image shows the height map determined by AFM (A) with the prominent protrusion representing the EF loop. The colored monomers represent the SD between the atomic models, and of the height measured by AFM. (C) Unraveling the force induced structural changes of the cytoplasmic surface by multivariate statistical analysis. Top left: purple membrane imaged at 80 pN. Top center: same membrane imaged at approximately 100 pN. Top right: at about 150 pN the EF loop is bent away while the shorter polypeptide loops of the cytoplasmic surface become visible. Bottom row: three conformations differing in their central protrusion are observed at approximately 180 pN. Topographs exhibit a vertical range of 1 nm and are displayed as relief tilted by 5°.

Dynamics of bR on purple membranes

Ando's group, Angew Chem Int Ed, 2011

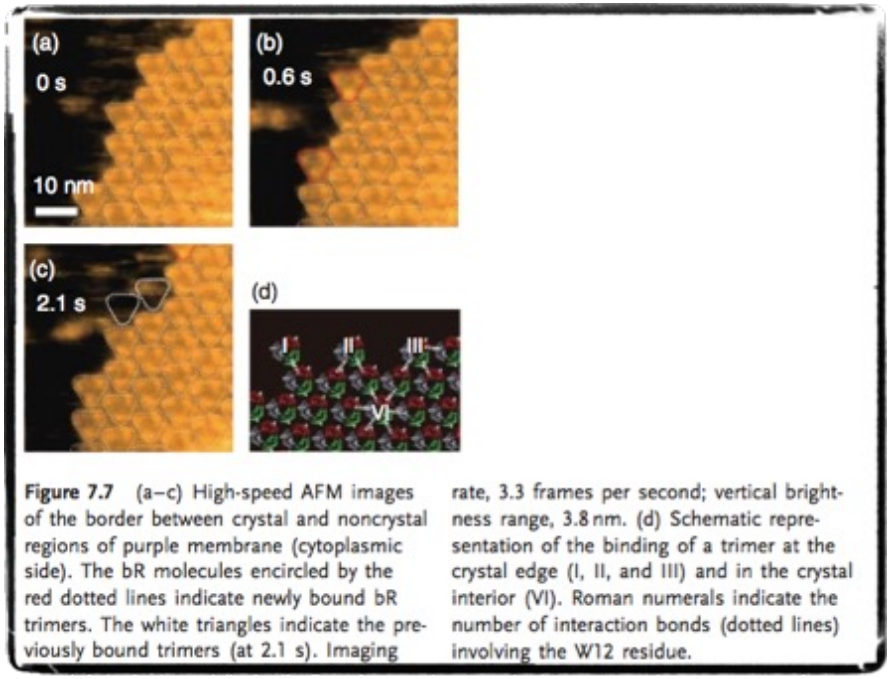

Figure 7.7 (a–c) High-speed AFM images of the border between crystal and noncrystal regions of purple membrane (cytoplasmic side). The bR molecules encircled by the red dotted lines indicate newly bound bR trimers. The white triangles indicate the previously bound trimers (at 2.1 s). Imaging rate, 3.3 frames per second; vertical brightness range, 3.8 nm. (d) Schematic representation of the binding of a trimer at the crystal edge (I, II, and III) and in the crystal interior (VI). Roman numerals indicate the number of interaction bonds (dotted lines) involving the W12 residue.

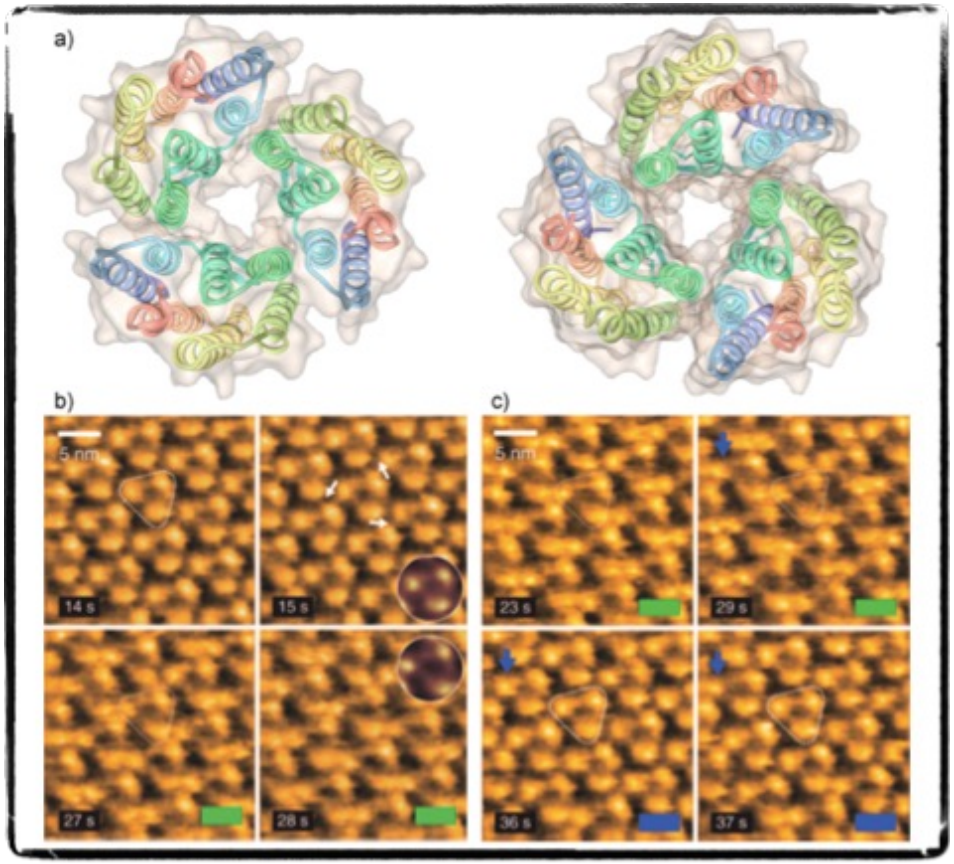

bR molecules with two binding partners associated for longer time periods to the array than proteins that had only one neighbor. Statistical assessment of the dissociation frequencies allowed the calculation of the **strength of a single bR–bR interaction of 1.5kBT (0.9 kcal/mol), resulting in a stability of about 5.4 kcal/ mol for the purple membrane arrays**, in good agreement with ensemble measurements by calorimetry

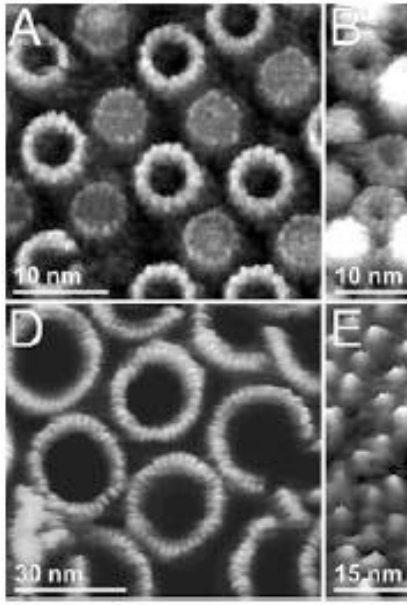

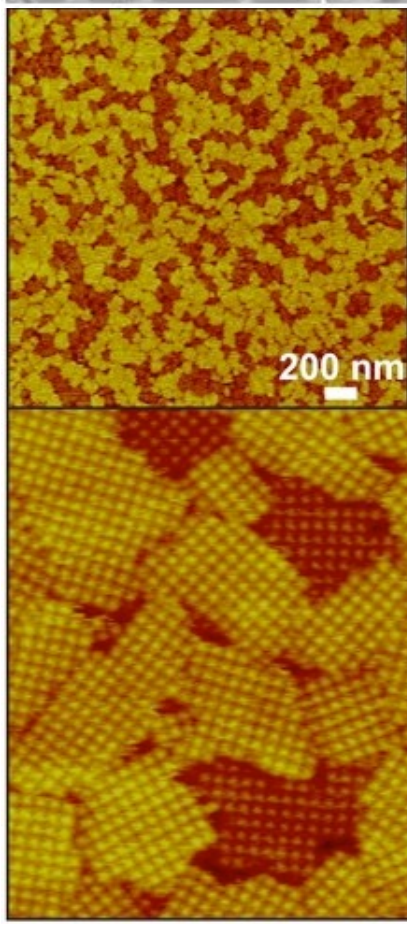

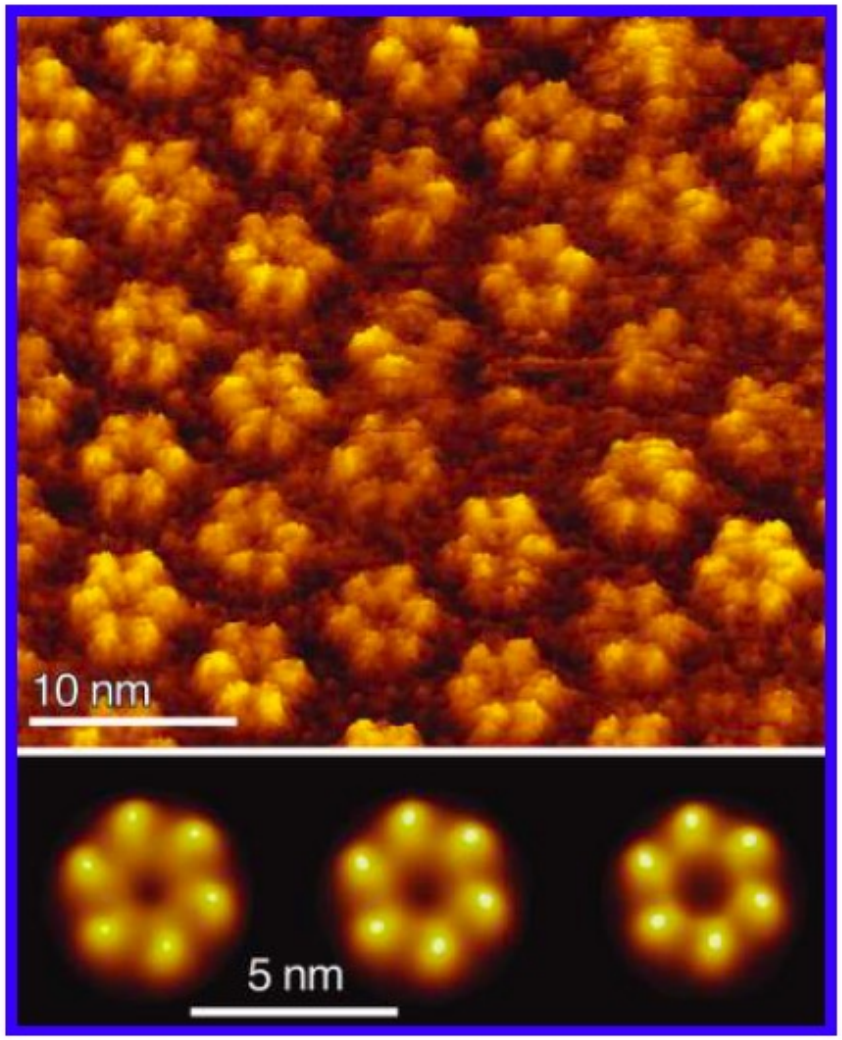

FIGURE 4: Watching communication channels at work. High-resolution AFM topograph showing the extracellular surface of Cx26 gap junction hemichannels. The gap junction membranes have been dissected with the AFM probe to expose their extracellular surface (*27*). The bottom row shows the conformational change of hemichannels in response to Ca^{2+}. The closed channels (left) switch, via an intermediate conformation (middle), to the open state (right) in the presence of 0.5 mM Ca^{2+}. Hemichannels in the bottom row represent correlation averages.

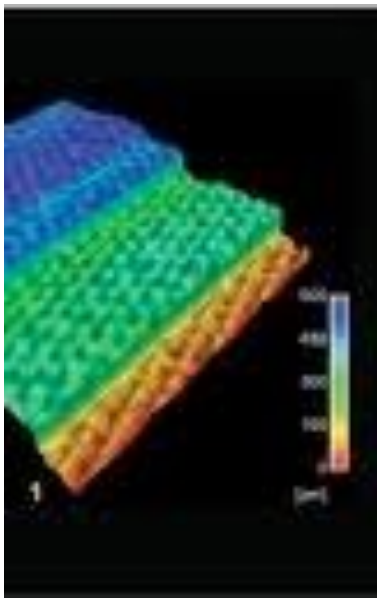

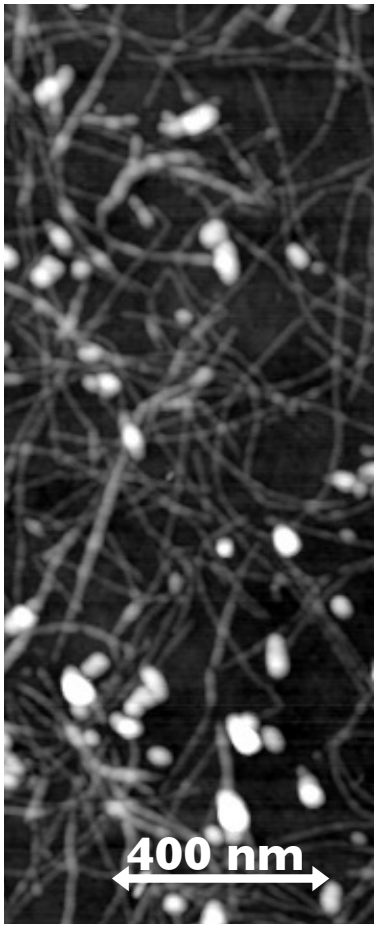

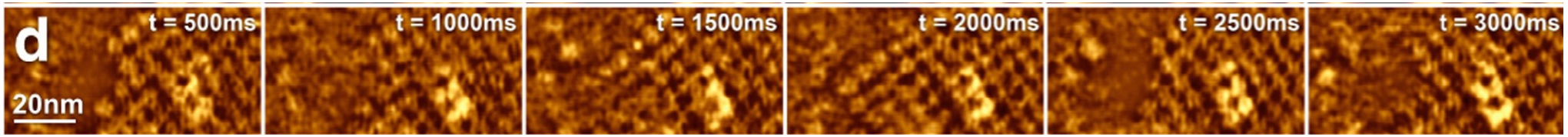

Using HS-AFM in contact mode, applying additional force s the junctional microdomains were dissected, revealing that the adhesion function of the proteins was cooperative: the entire membrane patches dissociated at once. From high spatial and temporal res. Assembly/dissasembly of auqaporin-0 and connexons to/from functional microdomains, with interaction strenght of -2.7 K_BT

HS-AFM on life cell

2.7 s/frame, with bright-field illumination

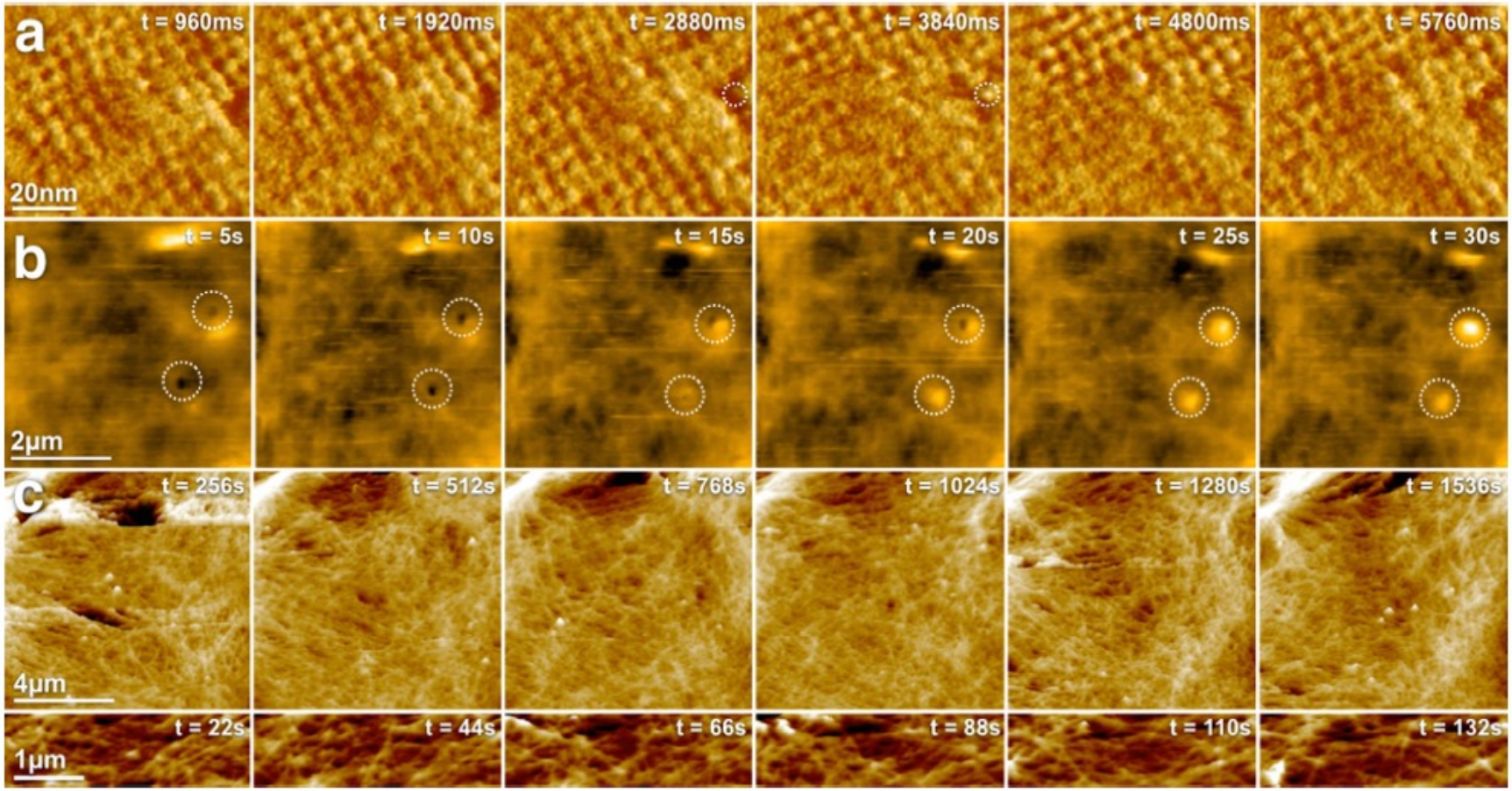

Fig. 2. HS-AFM applications on life cells. (a) High-resolution HS-AFM imaging of AQP0 in junctional microdomains in native eye lens cells. The dynamic association of individual AQP0 could be observed (outline). (b) Endocytosis events observed by HS-AFM on HeLa cells. (c) Dynamic PeakForce tapping imaging of the membrane cortex underneath the plasma membrane of 3T3 fibrobl

Colom, A., Casuso, I., Rico, F. and Scheuring, S. (2013) A hybrid high-speed atomic force–optical microscope for visualizing single membrane proteins on eukaryotic cells. Nat. Commun. 4.

Figure 5

Atomic force microscopy (AFM) images of the $\alpha_3\,\beta_3$ subcomplex at the C-terminal surface. (*a*) Schematic for F_1-ATPase. (*b*) Averaged AFM image obtained in nucleotide-free condition. (*c*) The C-terminal surface of crystal structure of a nucleotide-free $\alpha_3\,\beta_3$ subcomplex. (*d*) Simulated AFM image of panel *c*. (*e*) Averaged AFM image obtained in 1-mM AMP-PNP. (*f*) The C-terminal surface of crystal structure of an $\alpha_3\,\beta_3$ subcomplex obtained in ATP. (*g*) Simulated AFM image of panel *f*. (*h*) Successive AFM images showing counterclockwise rotary propagation of conformational change of an $\alpha_3\,\beta_3$ subcomplex at the C-terminal surface captured by high-speed AFM in the presence of 2 μM ATP, at 12.5 fps. The red circle marks the highest pixel position in each image. The color scale placed at the right-hand side of panels *b* and *f* indicate the *z*-scale for the respective images. Adapted with permission from Reference 99.

High-Speed AFM and Applications to Biomolecular Systems

Toshio Ando,[1,2] Takayuki Uchiashi,[1,2] and Noriyuki Kodera[2]

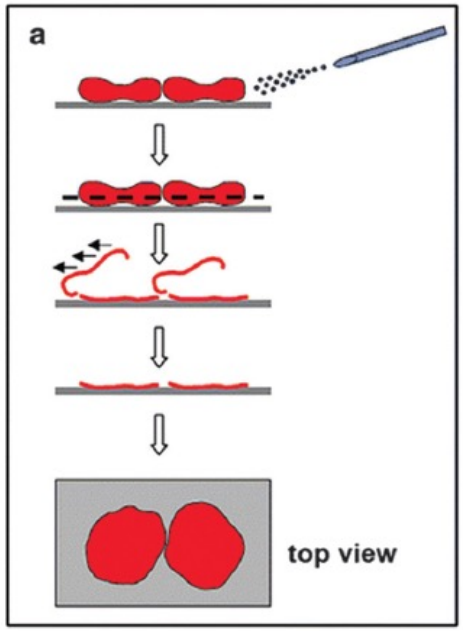

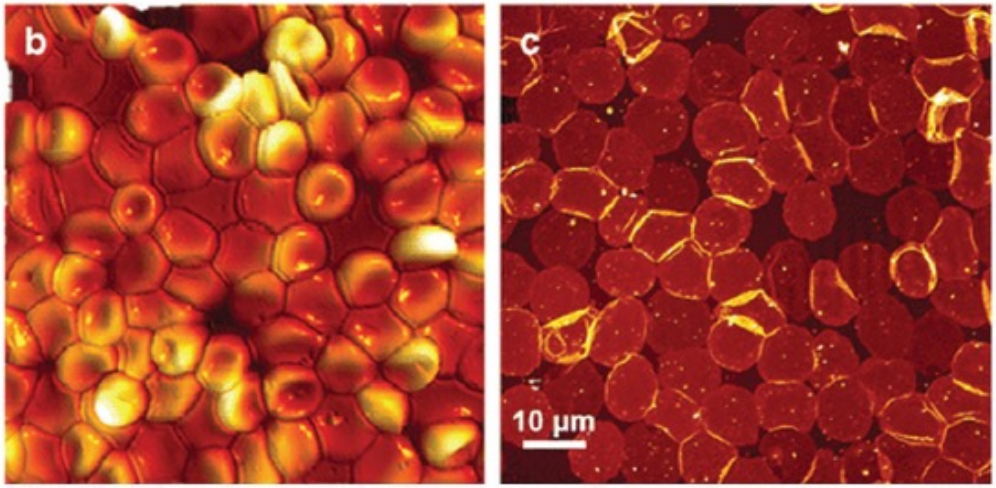

Fig. 11 Membrane preparation scheme. (a) RBCs are exposed to fluid flow-imposed shear stress to open the cells. (b) AFM images of RBCs attached to poly-L-lysine-coated glass. (c) Inside-out RBC membranes spread on the glass surface after shear stress. Adapted from ref. 91, Figure 1 with permission.

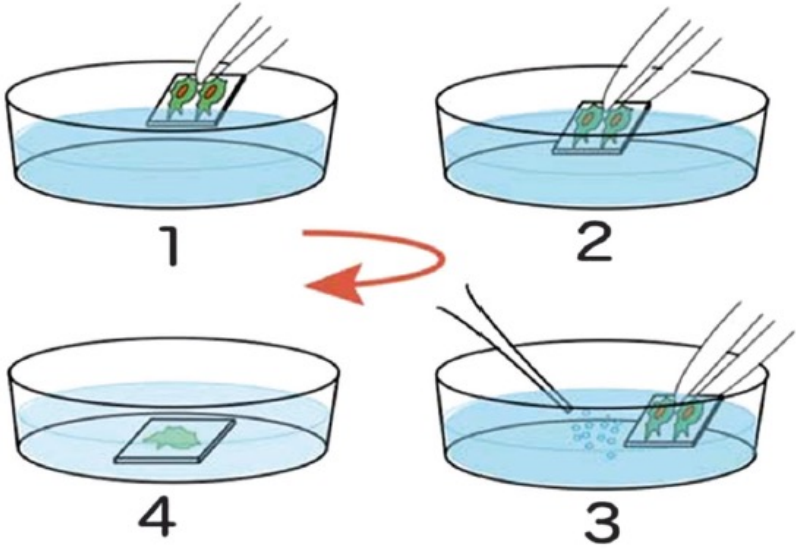

Fig. 12 Scheme for unroofing cells. The cells are washed three times in hypotonic HEPES-based mammalian Ringer's solution and subsequently unroofed by ultrasonic stimulation, which removes the apical cell membrane and the cytoplasm. Adapted from ref. 95, Figure 1 with permission.

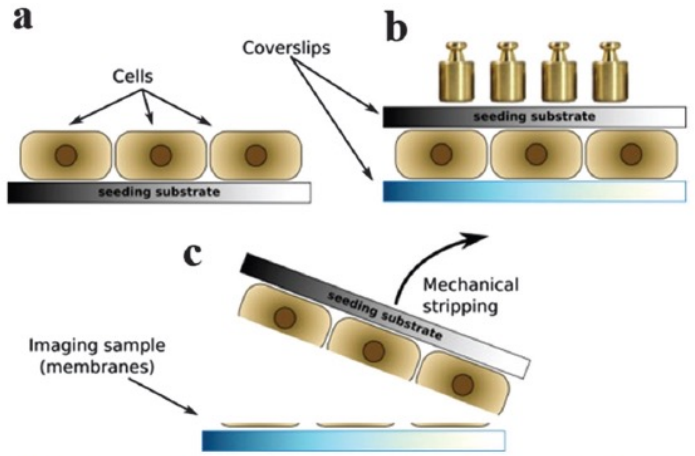

Fig. 13 Scheme of the preparation of the apical cytoplasmic side of membranes. (a) Cells are cultured on a seeding substrate. (b) A coverslip covers another side of the cells, and weights are placed on the seeding substrate. (c) Stripping the seeding substrate to leave the apical membranes for imaging. Adapted from ref. 97, Figure 1 with permission.

The $\alpha_3\beta_3\gamma$ subcomplex of F_1-ATPase (a part of ATP synthase) is the minimum complex for the full ATPase activity. About half the length of the long γ subunit is inserted into the central cavity formed by a ring-shaped $\alpha_3\beta_3$ where three α subunits and three β subunits are arranged alternately (1). Three ATP binding sites locate at the α-β interfaces, mainly in the β subunits. The $\alpha_3\beta_3\gamma$ subcomplex is a rotary motor (34, 48, 68, 115) (**Figure 5*a***). The γ subunit rotates in the stator $\alpha_3\beta_3$ ring driven by rotary hydrolysis of ATP at the three β subunits. The rotation occurs in the counterclockwise direction as viewed from the exposed side of the γ subunit (or from C-terminal side of $\alpha_3\beta_3$). In the ATPase cycle, three β subunits take different chemical states: ATP-bound, ADP-bound, and nucleotide-free (empty) states (1, 34). Each chemical state cyclically propagates over the three β subunits. Thus, there is strong cooperativity between β subunits.

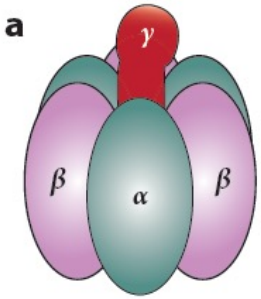

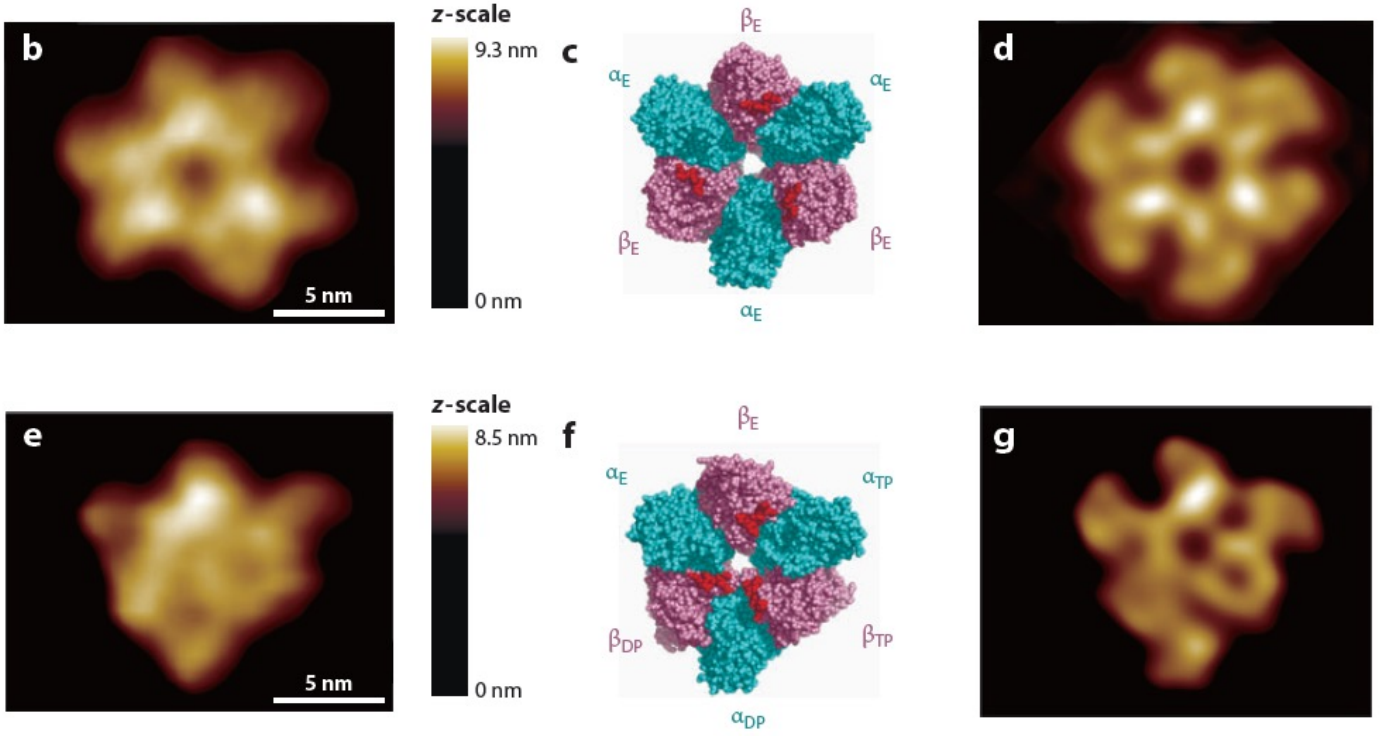

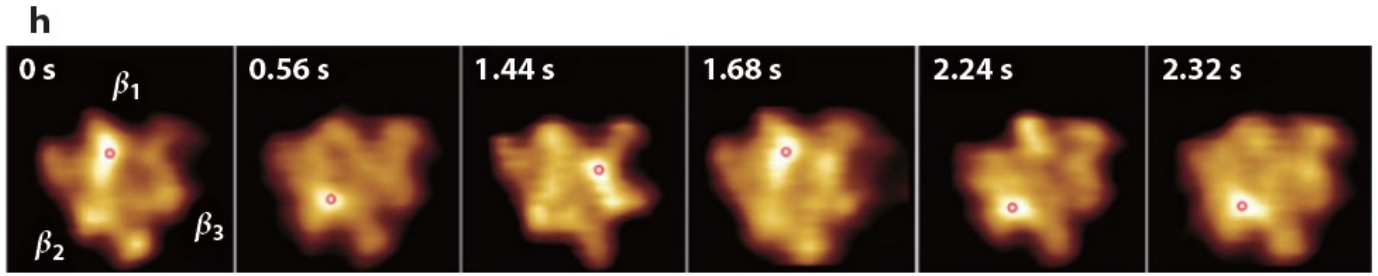

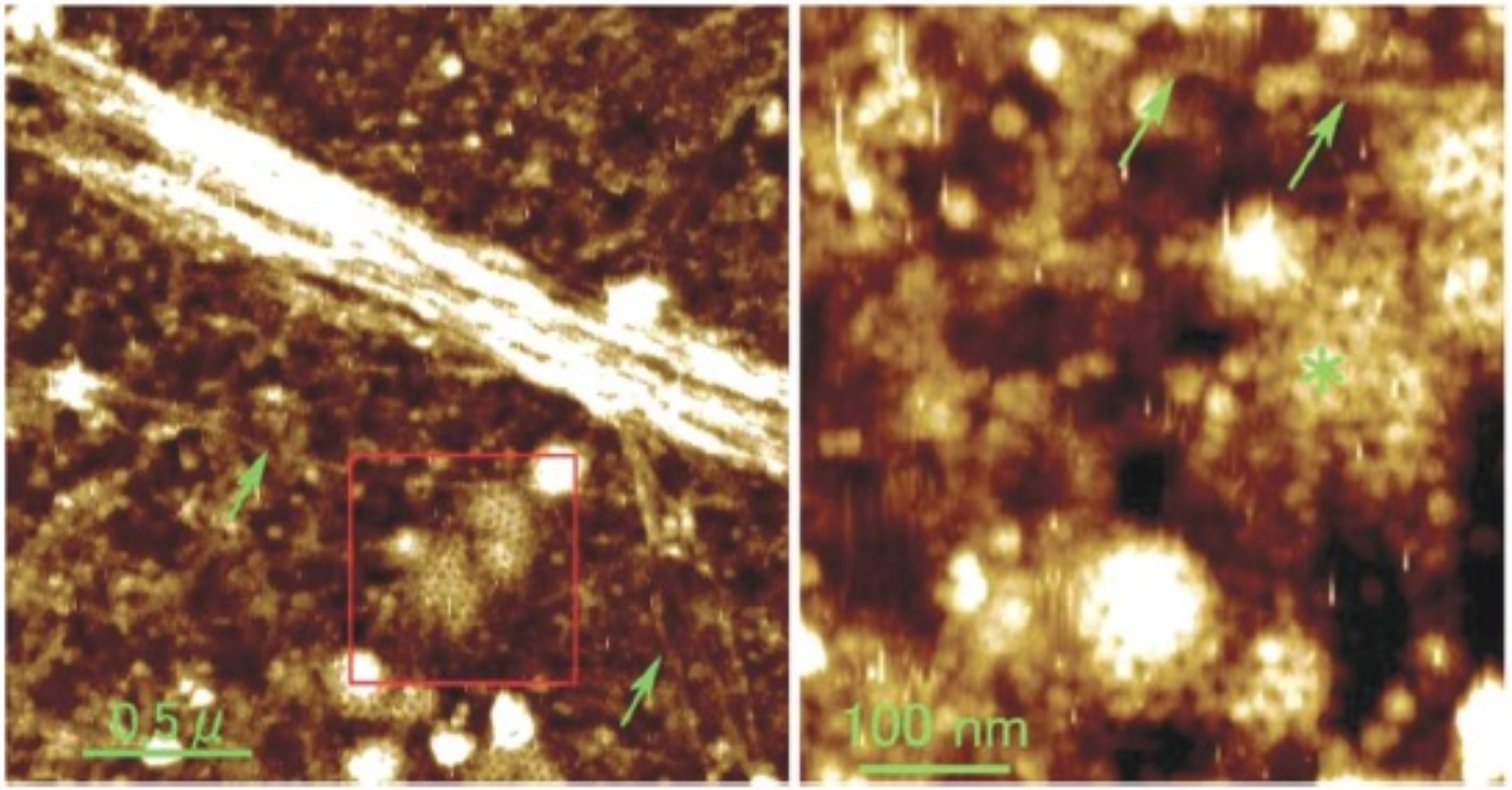

Fig. 18 AFM image of clathrin coats and actin filaments at the cytoplasmic surface of the plasma membrane. The right figure shows an enlarged view of the boxed area in the left figure. Clathrin-coated pits are clearly observed in the boxed area. Arrows indicate actin filaments. From ref. 95, Figure 6 with permission.

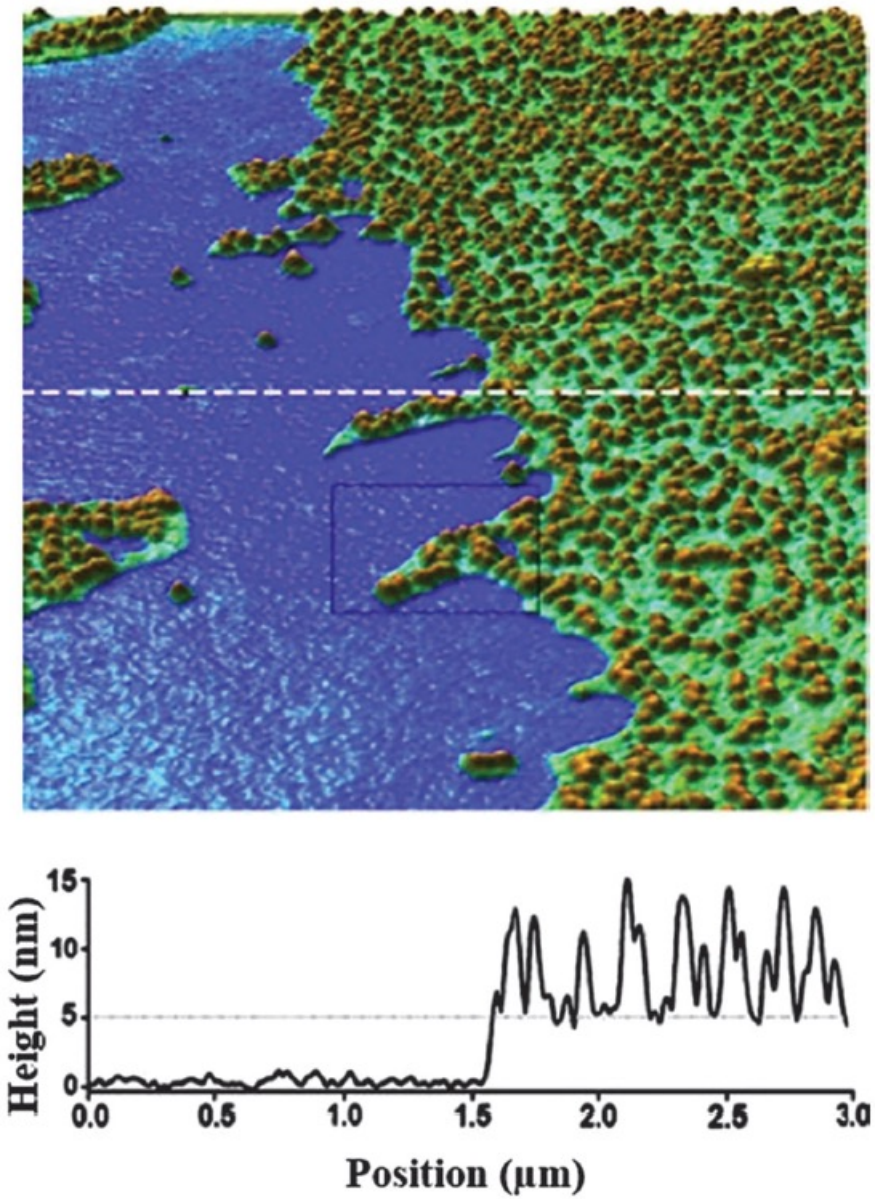

Fig. 17 AFM image of South African frog oocyte membranes (cytosolic side). Poly-L-lysine-coated glass (blue), the lipid bilayer membrane (turquoise), and the membrane proteins (brown). The height profile along the broken line is presented at the bottom. From ref. 91, Figure 6 with permission.

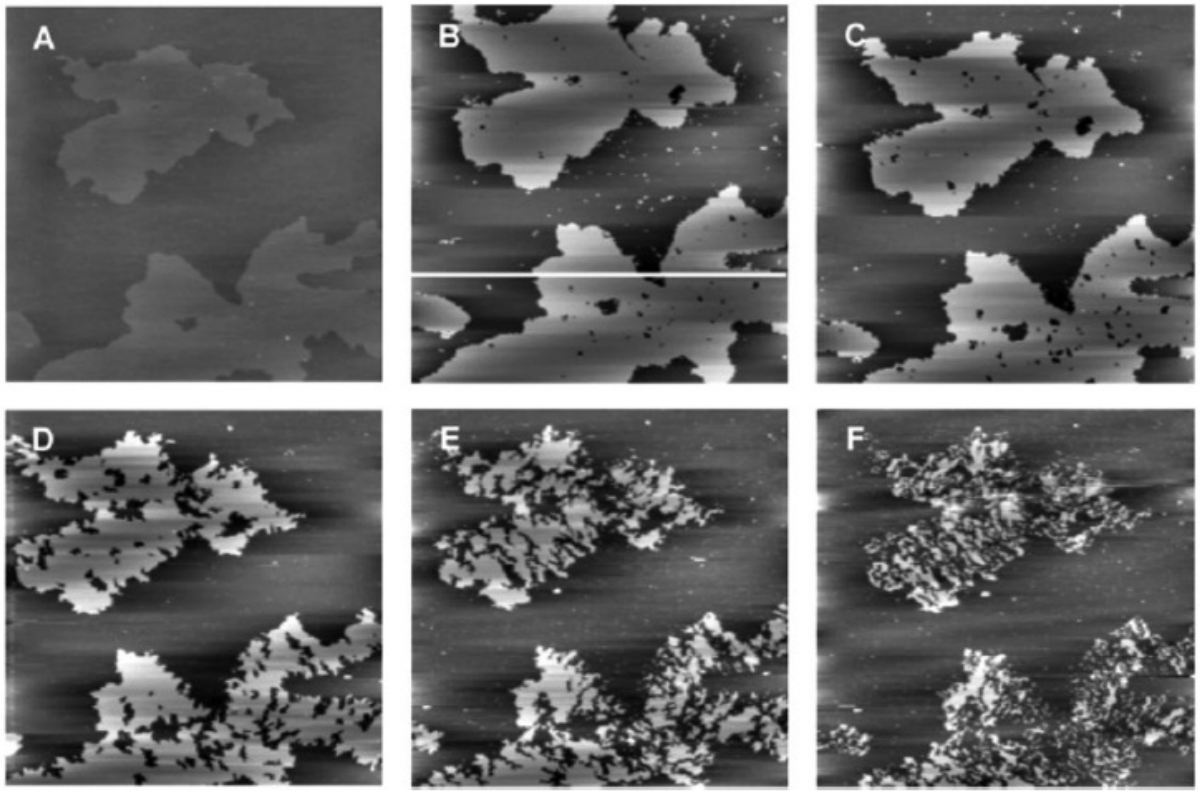

Fig. 14 Supported lipid membranes treated with TX-100. (A) An AFM height image (20 × 20 μm^2) of a mixed DOPC/DPPC bilayer prior to TX-100 addition. (B–F) Serial images after the addition of 0.48 mM TX-100 for 3.5 min (B), 10 min (C), 30 min (D), 60 min (E), and 90 min (F). Adapted from ref. 108, Figures 2A–F with permission.

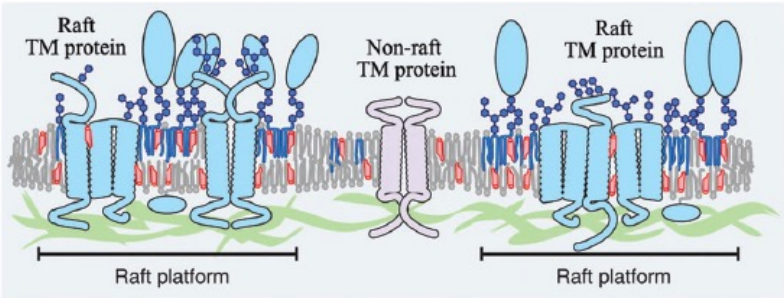

Fig. 3 Lipid raft domains in cell membranes. Adapted from ref. 25, Figure 2b with permission.